



Sustainable processing of Europe's low-grade sulphidic and lateritic nickel/cobalt ores and tailings into battery-grade metals (ENICON)

D1.1

Report on characterisation, surface chemistry, metal department/partitioning & mass balance for sulphides and laterites



Public

Authors:

Nivea Magalhães, University of Exeter

Fernando Prado Araujo, KU Leuven

Hannah S. R. Hughes, University of Exeter

Jens Andersen, University of Exeter

Rich Crane, University of Exeter

Philippe Muchez, KU Leuven

Date:

30-01-2025



This project has received funding from the European Union's EU Framework Programme for Research and Innovation Horizon Europe under Grant Agreement No 101058124

<https://enicon-horizon.eu/>

Deliverable Number	D1.1
Deliverable Name	Report on characterisation, surface chemistry, metal deportment/partitioning & mass balance for sulphides and laterites
Due Date of Deliverable	31-01-2025
Actual Submission Date	30-01-2025
Deliverable Lead Organisation	UNEXE
Dissemination Level	Public
Public Summary enclosed	No
Work Package	WP1 Forensic geometallurgy
No of Pages	56
Keywords	critical raw materials, battery metals, forensic geometallurgy, Ni-Co magmatic sulphides, Ni-Co laterites
In bibliography, this report should be cited as follows:	Nivea Magalhães, Fernando P. Araujo, Hannah S. R. Hughes, Jens Andersen, Rich Crane, Philippe Muchez. Report on characterisation, surface chemistry, metal deportment/partitioning & mass balance for sulphides and laterites (D1.1). ENICON - Sustainable processing of Europe's low-grade sulphidic and lateritic nickel/cobalt ores and tailings into battery-grade metals, 2025.



EXECUTIVE SUMMARY

The global demand for nickel (Ni) and cobalt (Co) is expected to increase significantly in the coming years.

Laterite deposits are a promising source of these metals. However, current processing methods (e.g., smelting or high-pressure acid leaching, HPAL) are energy-intensive and potentially environmentally hazardous. The ENICON project proposes a novel HCl-based processing route, but the complex mineralogy of laterite ores requires a thorough characterization of both inputs and outputs of the leaching stages. This study reveals the presence of Ni-bearing minerals like asbolane (Mn-hydroxide), nimitite (Ni-chlorite), and népouite (Ni-serpentine) in the high-grade samples, with an additional contribution from goethite, chlorite, and serpentine. Cobalt is mainly hosted by asbolane, with smaller amounts in goethite and chromite. HCl leaching effectively dissolves most Ni-Co-bearing minerals, but not chromite and this impedes full Co recovery. In-situ mineral chemistry assists in quantifying the metal department in the Ni-Co-bearing minerals.

The sulphidic ores studied in ENICON show sulphide minerals (pentlandite, pyrite, millerite) and oxides (magnetite, chromite) as the main Ni- and Co-bearing phases, with some Ni hosted in olivine. Despite the blending of different rock types in the feed material, the mineralogy and composition of the minerals tend to be relatively uniform. Although these minerals occur in low concentrations in the ore, mineral processing is used to concentrate these minerals, although concentrations of Co in this study are lower than what is observed in other Ni-Co concentrates from Finland. Analysis of the residues of HCl leaching of the sulphidic ore samples performed during ENICON showed mixed results, with half of the Ni and Co staying in the residue in one of the samples. A combination of oxidative and acid leaching performed showed good results on the removal of pyrrhotite in the material.

This forensic geometallurgical approach minimizes metal losses by investigating the causes of flowsheet underperformance.



Table of Contents

EXECUTIVE SUMMARY	4
List of abbreviations	7
1 Introduction	8
2 Materials and methods	10
2.1 Samples	10
2.2 Sample preparation	13
2.3 Bulk characterisation	13
2.3.1 XRF	14
2.3.2 ICP-OES	14
2.3.3 ICP-MS	15
2.3.4 Ni Fire Assay	15
2.3.5 XRD	15
2.3.6 Laser diffraction particle size analyser	16
2.4 Mineral/Particle characterisation	16
2.4.1 QEMSCAN	16
2.4.2 SEM-EDS	16
2.4.3 EPMA	16
2.5 Surface chemistry	17
2.5.1 Sequential extraction	17
2.5.2 XPS	18
3 Results and discussion	19
3.1 Task 1.1 – Ni/Co sulphide-bearing materials	19
3.1.1 Investigated flowsheet and sample information	19
3.1.2 Bulk particle size distribution (PSD)	20
3.1.3 Bulk geochemistry	20
3.1.4 Platinum-group element (PGE) geochemistry	22
3.1.5 Modal mineralogy	24
3.1.6 Mineral texture and chemistry of the sulphide ore	26
3.1.7 Surface chemistry (XPS)	30
3.1.8 Sequential extraction	34
3.1.9 Metal department and mass balance	36
3.2 Task 1.2 – Ni/Co laterite ores	38
3.2.1 Investigated flowsheet and sample information	38
3.2.2 Whole-rock geochemistry	39
3.2.3 Bulk particle size distribution (PSD)	43
3.2.4 Modal mineralogy	44
3.2.5 Mineral grain size	46
3.2.6 Mineral texture and chemistry	47



3.2.7	Metal department and mass balance.....	49
4	Future activities.....	54
5	Implications and Conclusions.....	54
6	References.....	55



List of abbreviations

BCR	European Community Bureau of Reference
BSE	Backscattered electron
EAF	Electric arc furnace
EDS	Energy dispersive X-ray spectroscopy
EPMA	Electron probe microanalyser
ICP-OES	Inductively coupled plasma optical emission spectroscopy
ICP-MS	Inductively coupled plasma mass spectroscopy
LAICPMS	Laser ablation inductively coupled plasma mass spectroscopy
MHP	Mixed hydroxide precipitate
MSP	Mixed sulphide precipitate
PGE	Platinum-group elements
QEMSCAN	Quantitative evaluation of minerals by scanning electron microscopy
REE	Rare earth elements
ROM	Run-of-mine – ore sampled from the mining stockpile
SEI	Secondary electron imaging
SEM	Scanning electron microscopy
WDS	Wavelength dispersive X-ray spectroscopy
XPS	X-ray photoelectron spectroscopy
XRD	X-ray diffraction
XRF	X-ray fluorescence spectroscopy



1 Introduction

The global demand for nickel (Ni) and cobalt (Co) is expected to increase, mainly due to their use in lithium-ion batteries (Gregoir and Van Acker, 2022; IEA, 2021). Although new battery technologies and recycling may help buffer this demand, mining and processing these metals will still be required for global decarbonization efforts. Hence, it is paramount to develop new technologies that decrease greenhouse gas emissions and environmental impacts of the Ni-Co supply chain. The Horizon Europe ENICON project (<https://enicon-horizon.eu/>) responds to this issue by developing a more sustainable HCl-based processing route for Ni/Co ores and enhancing the potential of these resources within Europe (Figure 1).

Nickel and cobalt deposits mainly occur in magmatic sulphide systems and laterites (Horn et al., 2021; Mudd and Jowitt, 2022). In the past, nickel extracted from Fe-Ni-Cu sulphides found in mafic or ultramafic intrusions or flows has represented 60 percent of the world's nickel production (Naldrett, 2004). While there are many magmatic bodies that contain Ni-Cu sulphide deposits worldwide, most are not economic either due to their size or their grade (Bates and Jackson, 1987). Due to their nature, these deposits also may contain other elements as byproducts, such as gold and platinum-group elements (PGE) at the g/t level and Co between the 0.1 to 0.3% (Barnes and Lightfoot, 2005). The main Fe-Ni-Cu deposits in Europe are located in Finland; the current active mines are Kevitsa and Talvivaara (Makkonen et al., 2017).

Lateritic deposits constitute more than half of the global nickel resources (Butt and Cluzel, 2013; Mudd and Jowitt, 2014) and currently represent most of the production (Mudd and Jowitt, 2022; USGS, 2024). However, the exploitation and processing of lateritic ores has the largest environmental footprint in the sector (Bartzas and Komnitsas, 2024, 2015; Jessup and Mudd, 2008; Mudd, 2010). Additionally, the mineralogy of laterites is often complex (Andersen et al., 2009; Elias, 2002; Gleeson et al., 2004; Tupaz et al., 2020; Villanova-de-Benavent et al., 2014) and directly affects the processing efficiency and its energy requirements (Stanković et al., 2022; Watling et al., 2011). Therefore, a thorough characterization (Figure 2) of both inputs and outputs of the processing stages is required to understand the mineral features that enhance or inhibit the efficient extraction of Ni and Co from laterites. The integration of this information with a life-cycle assessment (WP5) helps to fill the gaps and improve the environmental-economic impact of the newly proposed route. This report assesses the mineralogical constraints for extracting Ni and Co from sulphidic and lateritic ores in the HCl-leaching route investigated by the ENICON project. The bulk properties and mineralogy of both types of ores are compared to those from the solid residues after leaching to understand where losses are occurring.



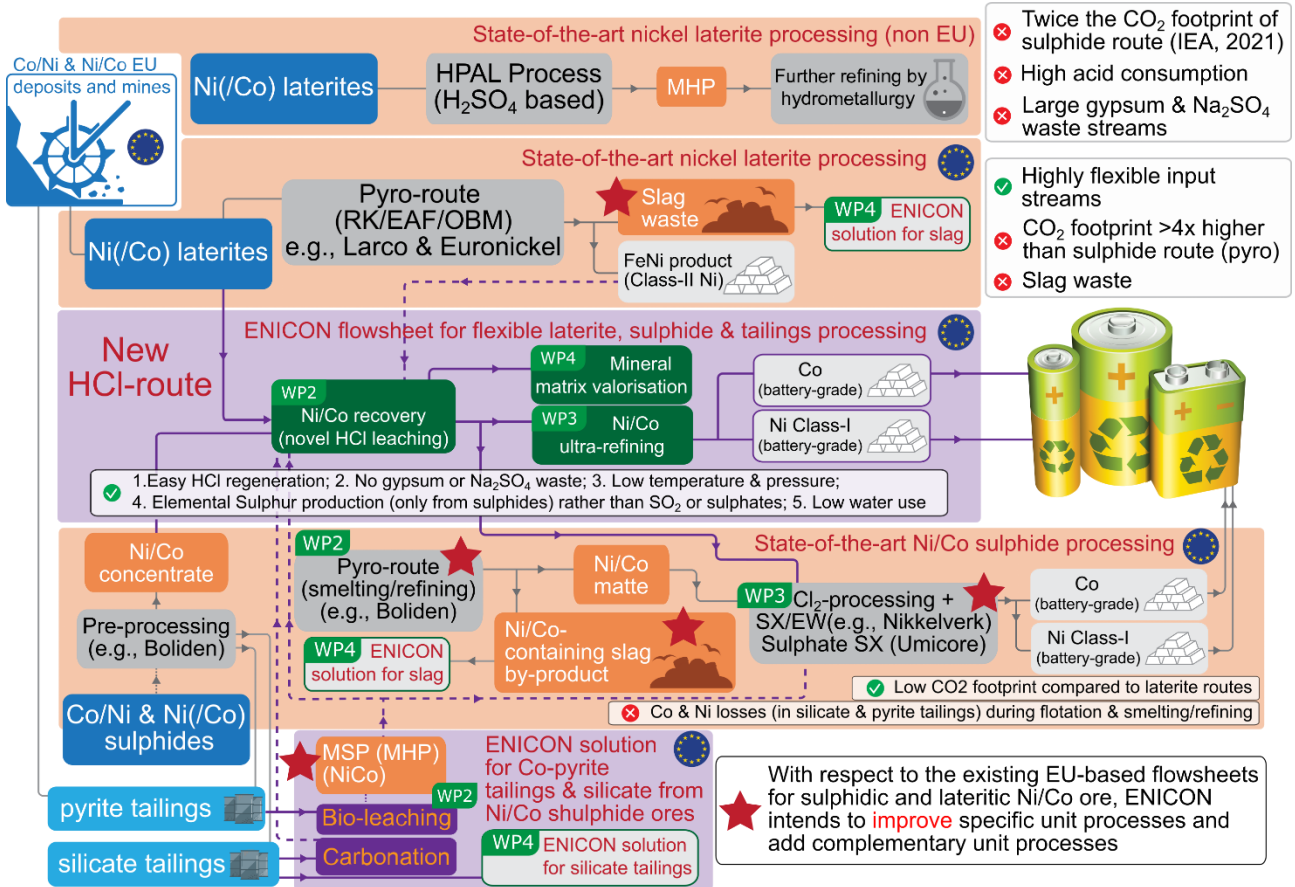


Figure 1: Diagram comparing the new HCl-route workflow with the state-of-the-art mining, recovery and refining route for Ni/Co deposits.

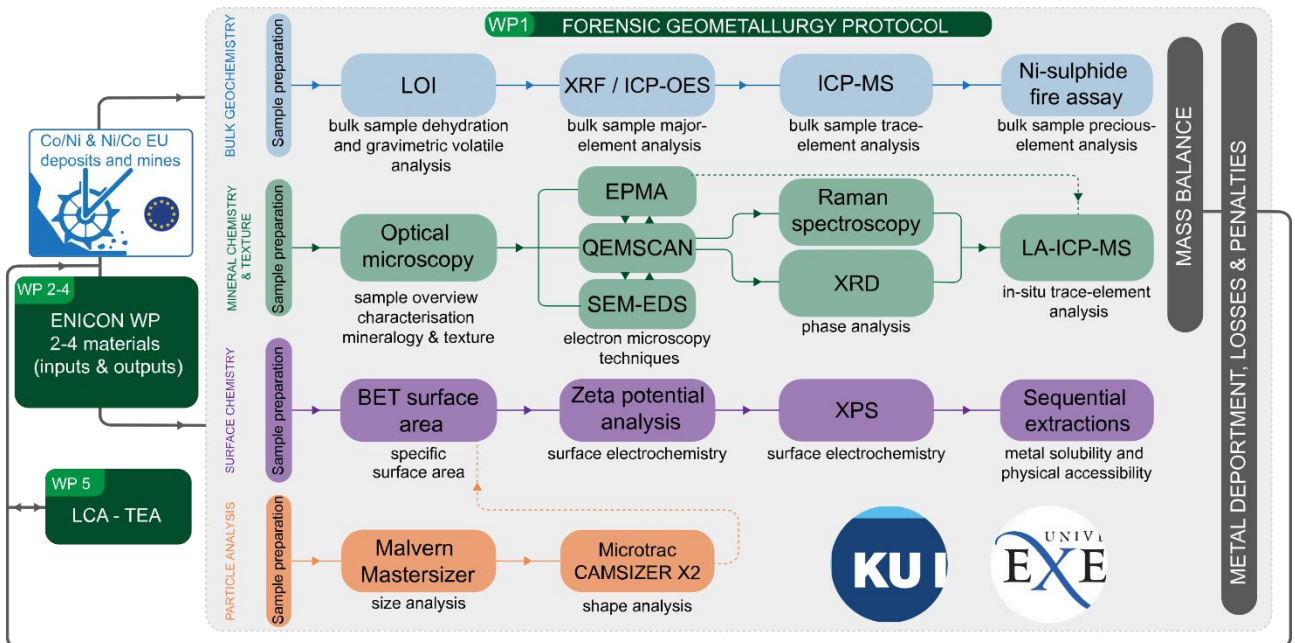


Figure 2: ENICON's forensic geometallurgy protocol & methodology. The interaction with LCA-WP5 is key in view of a joint optimisation of the economic & environmental performance of ENICON's mining & refining operations



2 Materials and methods

2.1 Samples

Sixteen laterite-related and twenty-one sulphide ore-related samples were investigated by the WP1 of the ENICON project.

Nineteen samples of Ni/Co-sulphide ore and subsequent processed materials were sampled from the Kevitsa Cu-Ni-(PGE) mine, located in Finland, which is operated by our project partner Boliden. The samples comprise materials ranging from the ore to concentrates (e.g. stockpile, flotation feed, tailings, slag, Figure 3; Table 1) that were collected directly in the processing plants with time constraints to assure. We analysed samples of leaching residues (acidic and oxidative leaching), and MHP/MSP produced by ENICON's WP2. Two additional samples provided by partner Finncobalt correspond to concentrate and tailings from different Co-bearing mines in Finland and have been used for comparison when relevant.



Figure 3. General aspects of some of the sulphide material samples studied, including the ore, slag, tailings, and concentrates.

Table 1. List of Ni/Co-sulphide materials from the HE ENICON project that were investigated in this report.

CODE	Running name	Raw material provider	Material description
ENICON001	Kevitsa ore - after cone crushers (stockpile)	BOMIN	Magmatic sulphide-type Ni-Co ore from Kevitsa mine (Finland) // Feed to ore stockpile, combined output of cone crushers
ENICON002A	Kevitsa Ni-Co concentrate (after filter press)	BOMIN	Ni/Co concentrate obtained from Kevitsa (Finland) after double flotation process
ENICON002B	Kevitsa Ni-Co concentrate (after thickener)	BOMIN	Ni/Co concentrate obtained from Kevitsa (Finland) after double flotation process



ENICON003	Hautalampi concentrate	Finncobalt	Ni/Co concentrate obtained from Hautalampi mine in Outokumpu (Finland)
ENICON004	Kevitsa pyrite tailings	BOMIN	Pyrite tailings from Kevitsa (Finland) after pyrite flotation process
ENICON007	Outokumpu copper mine oxidized pyrite tailings	Finncobalt	Historical oxidized pyrite tailings from the Outokumpu copper mine (Finland)
ENICON008	Kevitsa silicate tailings	BOMIN	Low-sulphur silicate tailings from Kevitsa (FI) after pyrite flotation process
ENICON011	Luikonlahti MHP	BOMIN	Mixed hydroxide precipitate obtained from bioleaching/oxidative leaching process of Luikonlahti/Kylylahti, produced by leaching of remaining BHP NEMO project
ENICON012	Luikonlahti MSP	BOMIN	Mixed hydroxide precipitate obtained from bioleaching/oxidative leaching process of Luikonlahti/Kylylahti, produced by leaching of remaining BHP NEMO project
ENICON013	Kevitsa MHP	BOMIN/WP2	Mixed hydroxide precipitate obtained from bioleaching/oxidative leaching process Kevitsa's pyrite tailings (performed in WP2)
ENICON014	Kevitsa MSP	BOMIN/WP2	Mixed sulphide precipitate obtained from bioleaching/oxidative leaching process Kevitsa's pyrite tailings (performed in WP2)
ENICON015	BOHA slag	BOHA	Fayalitic slag from pyrometallurgical processing on Ni/Co concentrates in Boliden Harjavalta, granulated (FI).
ENICON025A	Kevitsa Cu-concentrate (after filter press)	BOMIN	Cu concentrate obtained from Kevitsa (Finland) after flotation process
ENICON025B	Kevitsa Cu-concentrate (after thickener)	BOMIN	Cu concentrate obtained from Kevitsa (Finland) after flotation process
ENICON026	Kevitsa Cu tailings	BOMIN	Cu tailings obtained from Kevitsa (Finland) after Cu-flotation process
ENICON027	Kevitsa Ni-Co tailings	BOMIN	Ni tailings obtained from Kevitsa (Finland) after Ni-Co flotation process
ENICON031	Kevitsa ore - after mills	BOMIN	Magmatic sulphide-type Ni-Co ore from Kevitsa mine (Finland) // Feed to flotation plant, combined output of mills
ENICON033	Oxidative leaching residue of ENICON004	BOMIN/WP2	Leaching residue of Kevitsa HS tailings. Leaching residue after acid and oxidative leaching. (ENICON004 and ENICON030).
ENICON040	Acid leaching residue of ENICON004	BOMIN/WP2	Leaching residue of Kevitsa HS tailings. Leaching residue after acid leaching. (ENICON004 and ENICON030).
ENICON041	Leaching residue ENICON002B	WP2	Leaching residue of Ni-Co concentrate ENICON002B, after HCl acid leaching. Upscaled leaching test.
ENICON042	Leaching residue ENICON004	WP2	Leaching residue of ENICON004; from upscaled leaching test.

From the sixteen laterite-based samples, four are laterite ores, two are electric-arc furnace (EAF) slags, and two are ferronickel (FeNi) granules kindly provided by the industrial partners of ENICON, whereas the others are leaching residues produced by WP2 (Figure 4). The laterite ores consisted of run-of-mine (ROM) materials sampled from the stockpiles that feed the partners' processing plants. The process samples (slags and ferronickel granules) are the output of those processing plants. Additionally, the laterite ores were



subjected to HCl leaching (within WP2), and the solid residues after leaching under different conditions were also investigated (Table 2).

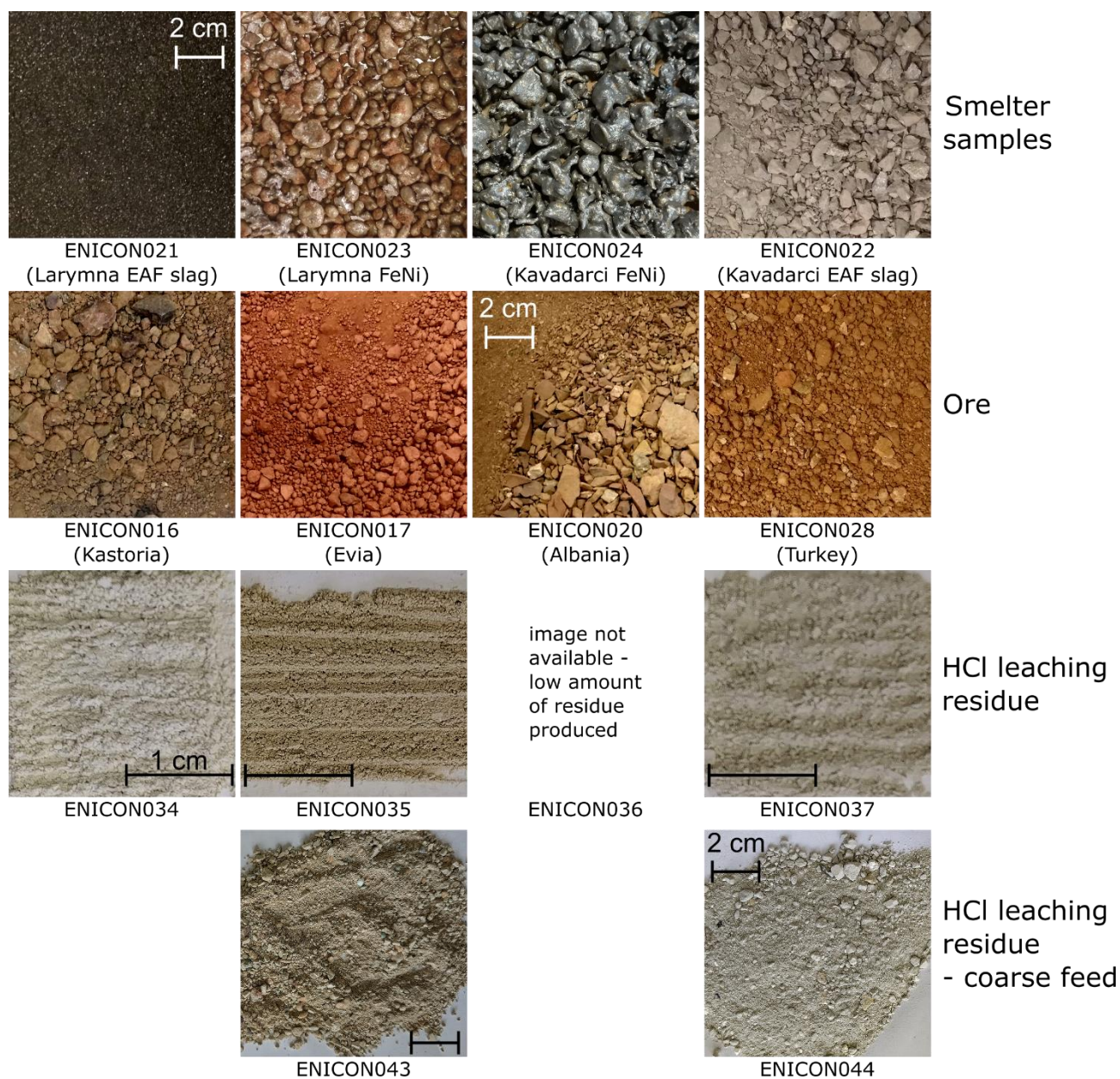


Figure 4: General aspects of the laterite-based samples studied, including smelting process output, lateritic ores sampled from stockpiles at the mine sites, and their residues after HCl leaching experiments. The scale bar is the same for all images in the same row.

Table 2: Laterite-based materials from the HE ENICON project and investigated in this report.

CODE	Running name	Raw material provider	Material description
ENICON016	saprolitic laterite Kastoria	Larco	Saprolitic laterite (low-grade) ore from Kastoria (Northern Greece)
ENICON017	limonitic laterite Evia	Larco	Limonitic laterite (low-grade) ore from Evia Island Greece
ENICON020	saprolitic laterite Albania	Euronickel	Saprolitic laterite (low-grade) ore Albania. 50-50 mixture of k-12 and Platinum deposits. Mixture is made to ensure that Fe-content is sufficiently high for the Euronickel process.



This project has received funding from the European Union's EU Framework Programme for Research and Innovation Horizon Europe under Grant Agreement No 101058124

<https://enicon-horizon.eu/>

ENICON021	EAF slag	Larco	EAF (fayalitic) slag from pyro-processing of laterite ores
ENICON022	EAF slag	Euronickel	EAF (fayalitic) slag from pyro-processing of laterite ores
ENICON023	Ferronickel	Larco	FeNi (Class II) product from pyro-processing (LARCO) of laterite ores
ENICON024	Ferronickel	Euronickel	FeNi (Class II) product from pyro-processing (Euronickel) of laterite ores
ENICON028	saprolitic laterite Turkey	Euronickel	Saprolitic laterite (high-grade) ore from Turkey
ENICON034	Leaching residue of ENICON016	WP2	Leaching residue of saprolitic laterite Kastoria Larco. Leaching residue after HCl acid leaching.
ENICON035	Leaching residue of ENICON017	WP2	Leaching residue of limonitic laterite Evia Larco. Leaching residue after HCl acid leaching.
ENICON036	Leaching residue of ENICON020	WP2	Leaching residue of saprolitic laterite Albania Euronickel. Leaching residue after HCl acid leaching.
ENICON037	Leaching residue of ENICON028	WP2	Leaching residue of saprolitic laterite Turkey Euronickel. Leaching residue after HCl acid leaching.
ENICON038	Leaching residue of ENICON016 + oxidant	WP2	Leaching residue of saprolitic laterite Kastoria Larco. Leaching residue after HCl acid and oxidative leaching.
ENICON039	Leaching residue of ENICON020 + oxidant	WP2	Leaching residue of saprolitic laterite Albania Euronickel. Leaching residue after HCl acid and oxidative leaching.
ENICON043	Leaching residue of coarse ENICON017	WP2	Leaching residue of limonitic laterite Evia Larco. Leaching residue after HCl acid leaching of ROM material.
ENICON044	Leaching residue of coarse ENICON028	WP2	Leaching residue of saprolitic laterite Turkey Euronickel. Leaching residue after HCl acid leaching of ROM material

2.2 Sample preparation

Different approaches were taken for the preparation of sulphide and the laterite ores, as sulphide ores were prepared at University of Exeter, UK, and the laterites at KU Leuven, Belgium. Due to the grain size additional comminution was not necessary for most samples collected at the Kevitsa Mine, and it was required only for the stockpile and slag samples. Approximately 10 kg of each was crushed using a jaw crusher and ground using a copper ring mill. The material was subsequently homogenized, and a rotary splitter was used to create splits of the material.

ROM ore materials were split about four times in a riffle splitter to produce a final sample mass of about 1kg. For each laterite ore, one of these final splits was dried in an oven at 40 °C to remove any moisture before being screened and jaw crushed (Retsch bb0) until a top size below 0.5 mm, whereas the remaining splits were stored in their raw format. The crushed material was again split, with half sent for HCl leaching experiments and the other half further split into smaller aliquots for characterisation analyses. The sample split for geochemical analysis was further ground to a powder (< 64 µm) using a tabletop planetary ball mill (Fritsch Pulverisette 5).

2.3 Bulk characterisation

For the quantification of all the samples' elemental composition, geochemical analyses were performed after digesting the samples using lithium metaborate fusion or four acid digestion procedures. Major and minor elements were measured by inductively coupled plasma optical emission spectroscopy (ICP-OES) in a



Varian 720ES system at the KU Leuven, Belgium. Trace elements were measured by inductively coupled plasma mass spectroscopy (ICP-MS) in an Agilent 7700x ICP-MS system at KU Leuven.

2.3.1 XRF

Bulk geochemical XRF analyses were performed with an ARL PERFORM'X 4200W spectrometer (Thermo Fisher) at the University of Liège (Belgium). The sample powders were initially roasted at 1000 °C for about 2h in a muffle furnace to obtain the loss on ignition (LOI) content by measuring the weight before and after ignition. Subsequently, 0.35 g (\pm 0.01 g) of sample was mixed with lithium metaborate (LiBO_2) flux in a sample:flux ratio of 1:11 and melted in a platinum crucible (the crucible was gently agitated during the procedure to homogenize the melt). The molten mixture was poured into a platinum mold to cast the glass disks to measure major elements. A standard program was applied for the measurement of the 10 major elements SiO_2 , TiO_2 , Al_2O_3 , $\text{Fe}_2\text{O}_{3\text{total}}$, MnO , MgO , CaO , K_2O , Na_2O , and P_2O_5 (reported as oxides). Calibration curves were obtained by measuring a series of 47 to 66 international standards (rock samples with a few minerals and soils).

2.3.2 ICP-OES

For the quantification of major and minor elements in the samples, two types of solutions were prepared and measured in an ICP-OES Varian 720ES system at the Department of Earth and Environmental Sciences of KU Leuven (Belgium). For calibration and validation purposes, two certified reference materials (GA and MA-N) were prepared and measured in the same way as the unknown samples, along with procedural blanks. The two types of solution procedures are described below.

Lithium metaborate (LiBO_2) fusion route: 100 mg of sample were mixed with 500 mg of LiBO_2 . The homogeneous mixture was placed in a graphite crucible and inserted into a pre-heated muffle furnace at 1000 °C for 10 minutes. The molten material inside the crucible was quickly poured into a polypropylene breaker with 50 mL of nitric acid (HNO_3 0.42M) in a magnetic stirrer. The solution is stirred for at least another 10 minutes. Once the sample dissolution was complete, the solution was transferred to a 50 mL plastic bottle. This final solution was measured by ICP-OES after 1/10 dilution.

4-acids (HNO_3 , HClO_4 , HF + HCl) digestion route: In this method, HNO_3 is used for the primary decomposition of a sample (powerful solvent for several minerals, especially sulphides and phosphates, and organic matter). HClO_4 is a very powerful oxidizing and dehydrating agent, it has a high boiling point and replaces other acids in their salts. HF reacts with silicates, forming the very unstable volatile silicon tetrafluoride SiF_4 , so that Si-free solution is obtained. HCl is used to create a more stable final solution.

100 mg of sample was added to a 15 mL Teflon Savilex vial with a rounded interior. 3 mL of HNO_3 (14M) is added to the vial, which is then closed with a screw cap and let stay overnight. The next day, the closed vial was placed on a hot plate and heated at 200 °C for about one hour. The vials were then opened, and the solution evaporated until a large single drop remained, after about 30 min while gently swirled a few times in between. 1 mL of HClO_4 (70%) was added to the vials, which were then covered and removed from the hot plate and let overnight at room temperature. The next day, the closed vials were heated at 240 °C for about one hour. One more time, the vials were opened, and the solution evaporated until a large single drop (about 0.5 ml) remained. 4 mL of HF (48%) was added to the vials and let to evaporate (uncovered) at 240 °C, swirling the vials occasionally, until a single viscous drop was left. White fumes (HClO_4) should be present at this late stage, meaning that all HF is gone. It is extremely important to get rid of any traces of HF because of its highly corrosive nature. Finally, 5 mL of HCl (2.5M) was added to the viscous droplet, the vial was swirled to homogenize the mixture, covered with the screw cap, and warmed up at 180 °C for at least 15 min to obtain a clear solution. Once a transparent solution was obtained, the vials were removed from the hot plate and let to cool down to room temperature. The cool solution was transferred to a volumetric flask and mixed with ultrapure water (Milli-Q) until a final volume of 50 mL was obtained.



2.3.3 ICP-MS

The concentration of trace elements in the solutions prepared using the 4-acids digestion route was measured in an Agilent 7700x ICP-MS system at the Department of Earth and Environmental Sciences of KU Leuven (Belgium). Before measurement, the solutions were diluted (1/5 dilution factor; 1 mL sample + 4 mL HNO₃ 5%) and spiked with an internal reference (0.1 mL of ISTD = Ir, Rh, Ge).

2.3.4 Ni Fire Assay

The nickel sulphide fire assay method with tellurium co-precipitation was used to measure the concentration of the platinum-group elements (PGE) in the whole rock samples. The Te co-precipitation step was necessary to pre-concentrate the PGE, ensuring their collection and removing other elements that could interfere with the measurement. The glasswork used in the preparation steps was cleaned with 'aqua regia' to remove any possible contamination. Although this method has higher costs, its cost-effectiveness is better than other methods because of its good recoveries and adequate detection limits (Rao & Reddi, 2000; Balcerzak, 2002). Only Os cannot be determined accurately since it forms volatile osmium tetra-oxide with HNO₃ during the final dissolution step (Juvonen et al., 2002).

Fifteen grams of powdered sample were mixed with 20 g of disodium tetraborate (Na₂B₄O₇), 10 g of sodium carbonate (Na₂CO₃), 3 g of clean quartz sand (SiO₂, acid purified and calcined p.a.), 3 g of sulphur powder (-325 mesh, 99.5% purity), and 5 g of nickel powder (APS 3-7 micron 99,9% metals basis).

The homogeneous mixture was transferred into a fire clay crucible and put into a muffle furnace at 1000 °C for 90 minutes. After cooling to room temperature (often on the next day), the crucible was broken and the nickel sulphide pellet that formed on the bottom of the crucible was cleaned of any residue of silicate glass matrix and collected. The pellet was then dissolved in 150 mL of hydrochloric acid (12M HCl) in a hot plate at 90 °C.

After the NiS pellet was completely dissolved, 5 mL of a tellurium solution (Te 1000 ppm) was added and quickly followed by 5 mL of tin(II)chloride (SnCl₂) solution to induce the precipitation of PGE. This step resulted in the formation of a black precipitate.

The precipitates were filtered in a vacuum pump system and collected in a 0.45 µm mix cellulose ester membrane. The membrane with the precipitate was then dissolved in 5 mL nitric acid (HNO₃) and 5 mL HCl and placed into a water bath at 90 °C for about one hour. After cooling back to room temperature, ultrapure water was added to reach the final volume of 50 mL. This solution was then diluted with HNO₃ 2% (1:1) to obtain the final solution for ICP-MS analysis.

The isotopes ¹⁰¹Ru, ¹⁰³Rh, ¹⁰⁵Pd, ¹⁰⁸Pd, ¹⁸⁵Re, ¹⁹³Ir, ¹⁹⁵Pt, and ¹⁹⁷Au were measured. To monitor the instrumental drift, ⁸⁹Y, ¹¹⁵In and ²⁰⁹Bi were used as internal standards. Calibration solutions for ICP-MS were prepared from a certified multi-element solution 'SQS-34E' along with procedural blanks (same workflow to unknowns but with no sample powder added) and 2 certified reference materials (UMT-1 and WGB-1 - Gupta, 1994).

2.3.5 XRD

Bulk mineralogical analyses by XRD were performed at two different institutions. The analyses of Ni/Co-sulphide samples were conducted at University of Exeter (Streatham Campus) in a Bruker D8 advanced XRD with a XE-T detector and Cu-Kα radiation source. Approximately 5g of each sample was placed in a glass holder and scanned with angles between 2θ between 5°-90° and steps of 0.02°. Subsequent data quantification through Rietveld refinement was obtained using GSAS-II software and utilizing mineral parameters available in the literature.

The analyses of laterite-related materials were performed with a D8 Advance diffractometer (Bruker), using a XE-T detector and Cu-Kα radiation source, at the commercial lab Qminerals (Belgium). A representative



subsample of 1.8 g was mixed with 0.2 g of corundum, used as an internal standard, and milled with ethanol in a McCrone Micronizing Mill. The slurry was spray-dried on a flat surface to avoid the preferred orientation of crystals (this step is important for the precise identification of phyllosilicates and clay minerals). Data quantification was obtained with the TOPAS software (Bruker) using the Rietveld refinement.

2.3.6 Laser diffraction particle size analyser

The particle size distribution analysis of the Ni/Co-sulphide ore was done at the University of Exeter using a Malvern Mastersizer 3000 coupled with a wet sample feeder module. Sample was added to the distilled water in the feeder until an obscuration around 10% is achieved. Each sample is run 5 times, and the results represent the average of these runs.

The bulk particle size distribution of the laterites was measured using a Beckman Coulter LS 13 320 laser diffraction particle size analyser coupled with an Aqueous Liquid Module (ALM) sample feeder at the Department of Earth and Environmental Sciences of KU Leuven (Belgium).

2.4 Mineral/Particle characterisation

2.4.1 QEMSCAN

Ore and leaching residue samples were mixed with graphite powder and mounted in epoxy resin before being measured in Fieldscan mode (10 µm spacing) in a Quantitative Evaluation of Minerals by Scanning Electron Microscopy (QEMSCAN) system at the Camborne School of Mines (CSM), University of Exeter, England. The instrument used was a Quanta 650F FEI (Thermo Fisher) field emission gun scanning electron microscope (FEG-SEM) with two energy dispersive X-ray spectroscopy (EDS) detectors (6030 SDD Bruker).

The sample was mixed with pure graphite powder to prevent particles from touching each other and to minimise the effect of differential settling. For the Ni/Co-sulphide materials, an extra step has been taken during preparation, as clumping of particles became an issue during sample preparation, and which could potentially be related to the usage of chemicals for flotation. Approximately 5g of homogenized sample was added to 800 mL of hot water with a drop of soap and stirred in the sonicator for 5 minutes. Subsequently it was filtered in a 12-22µm paper filter under vacuum. The procedure was repeated three times, and after the last one, the samples were put to dry in an oven at 55°C.

2.4.2 SEM-EDS

The Ni/Co-sulphide ore samples were imaged in a TESCAN Vega3 GMU scanning electron microscope (SEM) using secondary electron imaging (SEI) for investigation of particle morphology and backscattered electrons (BSE) to image mineral textures, using 10 kV and 15kV acceleration voltages, respectively, beam current of 18 nA, and 10-15 mm working distance. We used energy dispersive X-ray spectroscopy (EDS) for quick identification of the mineral phases present in the samples.

Laterite samples were imaged by BSE in a TESCAN Mira SEM to uncover the internal texture of the particles and measured by EDS to identify the elements present in each mineral phase. BSE images were captured with a 15 mm working distance, 20 keV acceleration voltage, and 1 nA beam current. For the EDS analyses, the beam current was adjusted to 10 nA.

2.4.3 EPMA

Quantitative *in situ* mineral chemistry was obtained by wavelength dispersive X-ray spectroscopy (WDS) in a JEOL JXA8200 electron probe microanalyzer (EPMA) at Camborne School of Mines, which is equipped with the Probe for EPMA software. Analyses on silicates and oxyhydroxides were carried out using a 15 nA



electron beam accelerated to 15 kV and a 5 μm spot size. Sulphide analyses were conducted using an electron acceleration of 15 kV, beam current of 20 nA, and a spot size of 0 μm .

Separate routines were calibrated for silicate, oxide, and sulphide minerals. For silicate and oxide minerals, wollastonite was used for Ca, diopside for Mg, almandine for Fe, Al and Si, orthoclase for K, jadeite for Na, chromium oxide for Cr, rutile for Ti, rhodonite for Mn, tugtupite for Cl, and apatite for P and F. V, Ni and Co were calibrated on pure metals. Si, Al, and Na were measured using a TAP crystal, Mg and F on TAPH, Ti, Ca, K, Cl, and P on PETJ, and Ni, Co, Fe, Mn, Cr, and V were measured using LIFH. All elements were measured in the $K\alpha$ line. For oxides and silicates, oxygen was calculated by charge balance to the measured cations under the assumption that all Fe is Fe^{2+} . Vanadium was corrected for interference from the Ti-K β line in the Probe software. For sulphides, arsenopyrite was used as a standard for As, pyrite for Fe and S, galena for Pb, pentlandite for Ni, sphalerite for Zn, and Cu and Co were calibrated in pure metals. As was measured on a TAP crystal, Fe, Ni, Co, Cu, and Zn on LIF, and S and Pb on PETH. Fe, S, Ni, Co, Cu, and Zn elements were measured on their $K\alpha$ line, Pb was measured on the $M\alpha$ line and As was measured on L β line. Matrix correction used the PRZ method to translate the raw signal into the composition of unknown samples.

Qualitative compositional maps were collected at 15 kV accelerating voltage, with 100 nA beam intensity for sulphides and 80 nA intensity for silicates, dwell times of 50ms, and pixel size dependent on the area to be mapped. Ni, As, Cu, and Co were obtained by WDS and any remaining elements by EDS.

2.5 Surface chemistry

2.5.1 Sequential extraction

The three-step sequential extraction BCR method (Davidson et al., 1998) was used to analyse samples from Kevitsa mine tailings (high and low sulphur tailings from Kevitsa, and tailings from Outokumpu). The first step is to extract the exchangeable fraction/acid soluble by adding 20 ml of acetic acid (0.11M) to 0.5g of dry sample in a 50 ml polypropylene centrifuge capped tube. The bottle was shaken for 16 hours at ambient temperature (approx. 24°C) on an end-over-end mechanical shaker operating at 40 rpm. The extract was separated from the solid residue by centrifugation (3000 rpm) and filtered (with 45mm 0.45 μm cellulose nitrate filter paper) into a polyethylene container and stored at 4°C for analysis. The residue was washed with 20 ml of distilled water and shaken for 15 min, centrifuged and the washings discarded.

To obtain the reducible fraction, we added 20 mL of 0.5 M hydroxylamine hydrochloride solution to each of the washed solids from the previous step. These were then loaded onto an end-over-end mechanical shaker and mixed for 16 hours. After, the samples were centrifuged at 3000 RPM for 10 minutes. After the supernatant was decanted and filtered using 0.45 μm PTFE syringe filters, we washed the remaining solid with deionized water and centrifuged again at 3000 RPM for 10 minutes. The supernatant was decanted and filtered using 0.45 μm PTFE syringe filters. The filtered supernatants were then acidified using concentrated nitric acid and refrigerated ready for dilution.

In the third step, we obtain the oxidizable fraction by 5 mL of 8.82 M hydrogen peroxide to each residue. These were put in a water bath at 65°C until near dryness. Another 5 mL of 8.82 M hydrogen peroxide was added using an auto-pipette. The samples were again left in a water bath at 65°C until near dryness. An auto-pipette was used to add 25 mL of the 1 M ammonium acetate solution to each sample. These were loaded into the rotary mixer and extracted for 16 hours. The samples were then centrifuged at 3000 RPM for 10 minutes. The supernatant was decanted and filtered using 0.45 μm PTFE syringe filters. The solid was washed using 10 mL deionized water and centrifuged again at 3000 RPM for 10 minutes. The supernatant was decanted and filtered using 0.45 μm PTFE syringe filters. The filtered supernatants were then acidified using concentrated nitric acid and refrigerated ready for dilution.



The residue after the oxidative leaching was digested with 4mL concentrated nitric acid, 3mL perchloric acid and 15 mL hydrofluoric acid to dryness for 16 hrs at increasing temperature from 90 to 160°C. The remaining material were taken up in 5mL of 5M hydrochloric acid at 70°C for 1 hr and diluted to 25mL with distilled water. The solutions were filtered and analysed with ICP-MS to measure the concentration of elements in the solutions. Total metal concentrations were calculated as the sum of the concentrations in the BCR extraction steps and in the residual digestion.

2.5.2 XPS

XPS is a technique based on the photoelectric effect, where the kinetic energy of electrons is measured. These electrons mostly come from the surface of the material (considering the standard XPS technique) and is sensitive to the chemical environment of the element. XPS is both a quantitative and qualitative technique.

XPS surface sensitivity comes from the fact that the electrons need to reach the detector with minimum interference (i.e. change in kinetic energy), and only the topmost electrons can do so. In a generalist approach, it is said that XPS detects around 10nm depth of the material.

XPS data was acquired using a Kratos Axis SUPRA using monochromated Al $K\alpha$ (1486.69 eV) X-rays at 15 mA emission and 12 kV HT (180W) and a spot size/analysis area of 700 x 300 μm . The instrument was calibrated to gold metal Au 4f (83.95 eV) and dispersion adjusted give a BE of 932.6 eV for the Cu 2p_{3/2} line of metallic copper. Ag 3d_{5/2} line FWHM at 10 eV pass energy was 0.544 eV. Source resolution for monochromatic Al $K\alpha$ X-rays is \sim 0.3 eV. The instrumental resolution was determined to be 0.29 eV at 10 eV pass energy using the Fermi edge of the valence band for metallic silver. Resolution with charge compensation system on $<$ 1.33 eV FWHM on PTFE. High resolution spectra were obtained using a pass energy of 20 eV, step size of 0.1 eV and sweep time of 60s, resulting in a line width of 0.696 eV for Au 4f_{7/2}. Survey spectra were obtained using a pass energy of 160 eV. Charge neutralisation was achieved using an electron flood gun with filament current = 0.4 A, charge balance = 2 V, filament bias = 4.2 V. Successful neutralisation was adjudged by analysing the C 1s region wherein a sharp peak with no lower BE structure was obtained. Spectra have been charge corrected to the main line of the carbon 1s spectrum (adventitious carbon) set to 284.8 eV. All data was recorded at a base pressure of below 9×10^{-9} Torr and a room temperature of 294 K. Data was analysed using CasaXPS v2.3.19PR1.0. Peaks were fit with a Shirley background prior to component analysis.

The X-ray photoelectron (XPS) data collection was performed at the EPSRC National Facility for XPS (“HarwellXPS”), operated by Cardiff University and UCL, under Contract No. PR16195.



3 Results and discussion

3.1 Task 1.1 – Ni/Co sulphide-bearing materials

Nineteen samples were investigated from the Kevitsa mine (Finland) ore processing chain and subsequent work by the ENICON WP2 team. These samples from Kevitsa represent different stages in the processing chain of Cu and Ni of the mine and includes samples of the stockpile, feed to flotation, Cu, Ni and S tailings, and Cu and Ni concentrates (Table 1). Further processed material by project partners during the work of WP2 has also been analysed, and comprise MHP/MSP samples, and both acid and oxidative leaching residues. Two sets of leaching residues have been analysed, a set of acidic and oxidative leaching of sample ENICON004 performed by project partners at Boliden (samples ENICON033, ENICON040; further details can be found in WP2 report), and HCl leaching performed at KU Leuven.

Two samples were sourced from other Co-bearing mines of Finland. ENICON007 corresponds to oxidized tailings from the Outokumpu Cu mine, and ENICON003 is a sample from the Ni-Co concentrates from Hautalampi. However, despite an initial negative asbestos test, asbestos was identified during analysis with the SEM in the imaging stage and further work was not conducted with this sample.

In total, twenty-one samples have been investigated following the proposed forensic geometallurgy protocol proposed by the ENICON consortium.

3.1.1 Investigated flowsheet and sample information

A simplified version of the Kevitsa flowsheet can be found in Figure 5. In summary, the ore is comminuted through a series of grinders prior to feeding it to flotation, where the sulphides are recovered. The first material to be recovered is the Cu-bearing sulphides (chalcopyrite and cubanite), followed by the recovery of Ni-bearing sulphides (pentlandite), and lastly, the separation of high and low S tailings. A more detailed version of the Kevitsa processing flowsheet can be found in the article by Musuku et al., 2016.

The “ore” sample ENICON001, collected from the Kevitsa stockpile, is a composite of different rock types that are blended during the grinding process. These comprise both igneous and metamorphic rocks from the Kevitsa Igneous Complex.

While all samples have been analysed, particular emphasis has been placed on the Ni-Co concentrate (ENICON002B) and the high S tailings (ENICON004) for leaching experiments within the context of ENICON’s WP2, as these are likely to contain the highest amounts of Ni and Co within the processing chain. The low S tailings (ENICON008) were the target for creation of pathways for matrix valorisation by WP3, however, these samples were not available for analysis prior to the closing of this report and will not be further discussed.

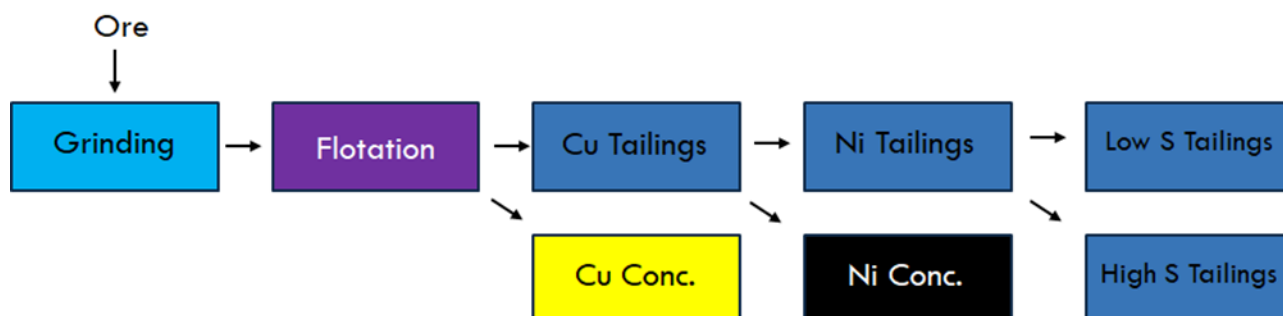


Figure 5. Simplified schematics of the processing flowsheet of the Kevitsa Mine, Finland, modified after Musuku, Muzinda and Lumsden, 2016.



3.1.2 Bulk particle size distribution (PSD)

The ENICON samples (excluding ENICON001 and ENICON015, which were comminuted at UNEXE and are not reported here) present P80 between 80 and 90 μm , and P10 between 4 and 12 μm (Figure 6); these samples are relatively homogeneous in grain size. The residue after oxidative leaching (ENICON033) presents slightly finer grain sizes (P80 of 18 μm and P10 of 5 μm), which is consistent with further grinding done by our project partners prior to leaching.

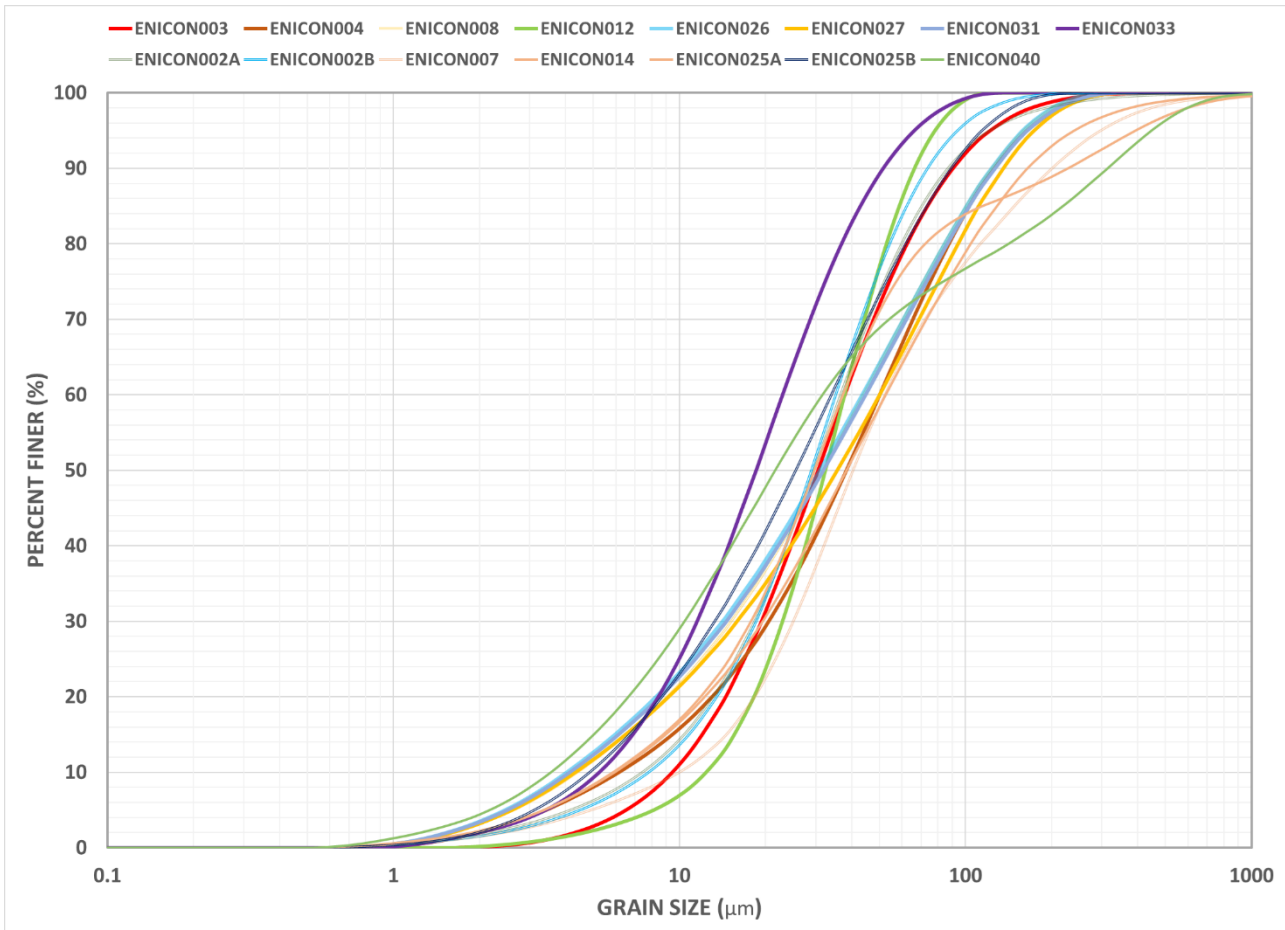


Figure 6. Particle size distribution (PSD) of the material sampled at the Kevitsa mine and leaching residues.

3.1.3 Bulk geochemistry

The bulk geochemistry data (Table 3; 4; 5) shows that the ore material has a relatively low concentration of Ni and Co (ENICON001), when compared to the enrichment after the process of concentration has been achieved (ENICON002A and ENICON002B). The composition of the ore clearly highlights the mafic-ultramafic nature of the sample, with high MgO and Fe_2O_3 , although the sample is a blend of different rock types from Kevitsa. Negative LOI (i.e., gain on ignition) in the slag samples is due to oxidation, likely of iron, at high temperatures (Vandenberghe et al., 2010).

We have observed no clear correlation between increase in concentration of Ni and Co in the Kevitsa (Figure 7) samples with the presence of other elements, as their variation can be explained solely by the processing flowsheet of the mine. The sample from the Hautalampi Ni/Co concentrate shows the highest Co concentration among all samples, with a value of up to 2.5 wt.%.



This project has received funding from the European Union's EU Framework Programme for Research and Innovation Horizon Europe under Grant Agreement No 101058124

<https://enicon-horizon.eu/>

The sample of the oxidized pyrite tailings from Outokumpu (ENICON007) shows a much lower concentration of sulphur and metals when compared to Kevitsa's high S and low S tailings (ENICON004, ENICON008).

The two sets of MSP and MHP samples (ENICON011, 012 from Luikonlahti, and ENICON013, 014 produced by WP2 of the ENICON project) have distinct chemistry. The first set is richer in cobalt (~12wt.%), the second set is richer in nickel (up to ~40%).

The analyses of the leaching residues produced by WP2 are presented in Table 4; low totals are likely due to the high concentration of metals (presented in Table 5) and sulphur. The acidic and oxidative leaching of high S tailings (ENICON004) show that there is a progressive loss in Fe with each step, as the initial Fe₂O_{3t} concentration is measured at 45.5 wt.%, while at the last stage (ENICON033) it is 13.5 wt.%, as expected in such procedure. Both concentrations of Ni and Co are lower in the residues than in the initial sample, reflecting the metal extraction during leaching. There is an enrichment in SiO₂, CaO, MgO, and sulphur in the residues when compared to the initial sample, likely related to the enrichment of silicates in the sample.

The HCl leaching residue of the same sample, ENICON042, shows a significant enrichment in SiO₂ and MgO when compared to the initial sample, while there is a drastic reduction in the concentration of Fe₂O_{3t}. The concentration of Ni and Co in the residue is also considerably lower than in the input sample. However, sample ENICON041, which is the residue resulting from leaching of sample ENICON002B (Ni concentrate), shows very high Ni and Co concentrations (7.4 wt.% and 0.4 wt.%, respectively), albeit lower than in the original sample. The concentration of sulphur in the sample (> 35 wt.%) is significantly higher than in the original sample. This information suggests that much of the metal budget of the Ni concentrate has remained in the residue.

Table 3. Whole rock composition of Kevitsa samples, in wt.%, measurement by XRF.

Composition measured by bulk geochemical analysis (XRF)																
sample	SiO ₂	TiO ₂	Al ₂ O ₃	Fe ₂ O _{3t}	MgO	MnO	CaO	K ₂ O	Na ₂ O	P ₂ O ₅	Ni%	Co%	Cu%	Ox_sum	LOI	total
ENICON001	47	0.3	4.3	12.3	19.7	0.2	12.2	0.2	0.1	0	0.2	0	0.3	96.8	2.5	99.2
ENICON002A	11.9	0.1	0.9	48.2	6.1	0	1.7	0	0	0	10	0.7	2.8	82.3	13.5	95.8
ENICON002B	11.7	0.1	0.8	49.8	6.1	0	1.7	0	0	0	11.1	0.8	2.8	84.8	11.4	96.2
ENICON003	9.5	0	1	52.3	4.4	0	0.9	0	0	0	8.3	2.5	1.8	80.8	13.1	93.8
ENICON004	25.8	0.1	2	45.4	12	0.1	5.2	0.1	0	0	1.1	0.1	0.3	92.2	7.1	99.3
ENICON007	67.6	0	2.1	11.4	4.7	0.1	2.2	0.3	0	0	0	0	0.1	88.6	9.3	97.8
ENICON008	47.9	0.3	4.3	11.1	20.6	0.2	12.4	0.2	0.2	0	0.1	0	0	97.3	2.2	99.5
ENICON015	35.3	0.2	3	54.8	9.2	0.1	2	0.5	0	0	0.1	0.3	0.2	105.7	-5.4	100.3
ENICON025A	8.5	0.1	0.8	32.3	4.2	0	2.1	0	0	0.1	1.2	0.1	38.6	88	12	100
ENICON025B	8	0.1	0.8	33.6	4.1	0	2.1	0	0	0.1	1.1	0.1	40.9	90.8	12	102.8
ENICON026	47.1	0.3	4.1	12.1	20.5	0.2	12.3	0.2	0.1	0	0.2	0	0.1	97.1	2.2	99.3
ENICON027	47.4	0.3	4.2	11.5	20.3	0.2	12.2	0.2	0.2	0	0.1	0	0	96.6	2.1	98.7
ENICON031	46.4	0.3	4.2	12.5	19.9	0.2	12	0.2	0.2	0	0.2	0	0.3	96.4	2.4	98.8

Table 4. Whole rock composition of the leaching residues produced by WP2, measurement by Li-fusion method.

	SiO ₂ wt%	TiO ₂ wt%	Al ₂ O ₃ wt%	Fe ₂ O _{3t} wt%	MgO wt%	MnO wt%	CaO wt%	K ₂ O wt%	Na ₂ O wt%	P ₂ O ₅ wt%	Cr ₂ O ₃ wt%	Total wt%
ENICON033	39.5	0.3	1.8	13.5	13.7	0.1	11.1	0.1	0.3	0.02	0.3	80.7
ENICON040	40.4	0.3	2.0	30.4	13.7	0.1	10.2	0.1	0.3	0.02	0.4	97.9
ENICON041	23.7	0.1	0.6	16.1	8.8	0.0	2.9	0.0	0.1	0.01	0.1	52.5
ENICON042	55.1	0.3	2.5	6.9	18.8	0.1	9.6	0.1	0.5	0.00	0.2	94.1



Table 5. Minor and trace element composition of elements of interest in sulphidic ores and associated leaching residues (bdl = below detection limit, n.a. = not analysed).

	Ni ppm	Co ppm	Cu ppm	S ppm	Pb ppm	Sc ppm	V ppm	Zn ppm	As ppm
ENICON001	1873.8	122.8	3052.4	13580.3	2.5	52.8	154.3	54.0	0.5
ENICON002A	72917.1	3861.9	19258.7	237607.9	34.2	7.0	28.1	n.a.	13.2
ENICON002B	77345.8	4312.3	17848.4	244042.5	33.7	7.8	28.9	n.a.	20.9
ENICON004	9439.0	434.3	2069.5	160402.7	15.6	22.5	81.6	76.0	3.4
ENICON007	481.0	565.8	1308.4	44801.9	20.5	52.8	154.3	54.0	0.5
ENICON008	905.9	68.8	362.1	6954.3	4.1	48.0	142.9	44.0	0.4
ENICON011	119630.2	183101.8	77.0	31201.0	5.2	3.4	0.7	n.a.	13.9
ENICON012	120268.3	187205.7	124.2	207448.7	2.5	bdl	bdl	n.a.	12.5
ENICON013	425386.7	18041.1	251.7	47114.7	139.7	2.2	bdl	n.a.	1.3
ENICON014	407379.2	16303.8	122.2	234107.6	33.4	0.6	bdl	n.a.	1.0
ENICON015	1277.4	1455.1	1717.2	2967.0	33.8	8.6	48.1	234.0	0.3
ENICON025A	6841.3	342.1	204216.9	217930.6	30.1	10.2	39.9	n.a.	2.4
ENICON025B	6386.1	329.0	211059.0	223915.1	33.1	9.2	37.0	n.a.	4.1
ENICON026	2072.6	123.2	516.0	11305.5	2.9	47.1	138.9	46.0	0.5
ENICON027	996.0	73.0	376.4	9197.9	3.8	46.8	141.0	45.0	0.5
ENICON031	2157.5	128.6	3745.7	14571.2	5.4	47.4	138.1	51.0	0.4
ENICON033	3239.5	147.7	2654.6	131380.3	142.7	32.1	88.3	109.0	23.1
ENICON040	18151.7	733.2	4827.2	108012.1	32.0	28.2	78.8	108.0	11.5
ENICON041	72816.2	4190.3	1937.9	353223.1	9.5	12.3	32.5	20.0	12.8
ENICON042	3432.3	179.8	341.0	54139.2	1.1	40.7	107.8	38.0	0.5

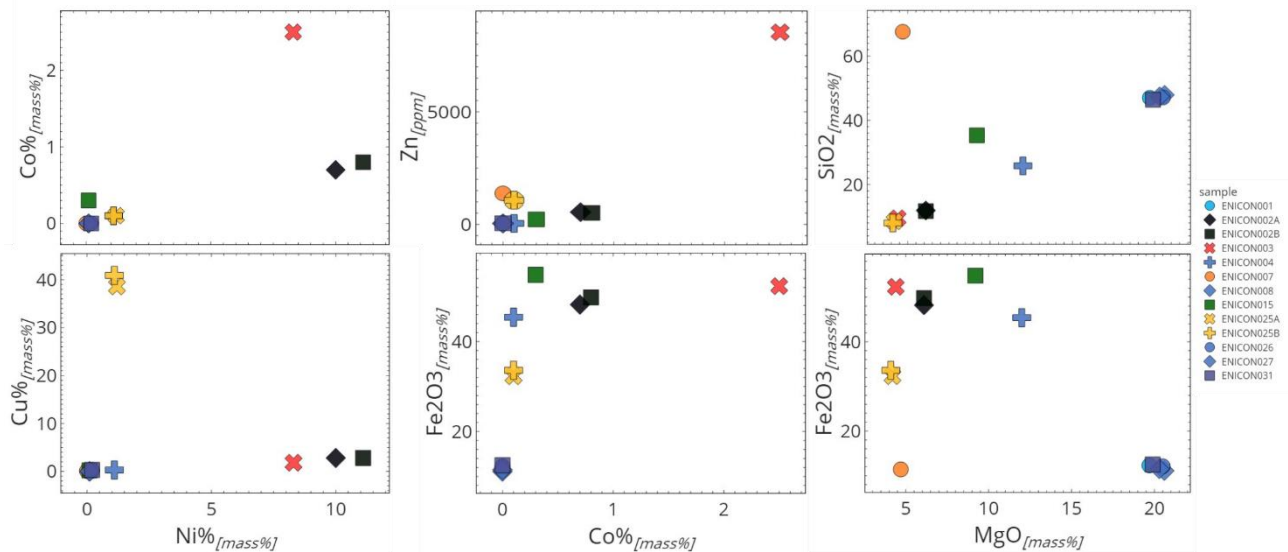


Figure 7. Elemental diagrams showing the chemical variation of the Kevitsa, Outokumpu, and Hautalampi samples.

3.1.4 Platinum-group element (PGE) geochemistry

Platinum-group element (PGE) concentrations were measured in six samples across the processing chain, from the ore to the Cu and Ni concentrates (Figure 8). We observe a consistent pattern and concentration in the ore and in the tailings (Ni, Cu, and low S; ENICON001, ENICON027, ENICON026, ENICON008), despite the removal of sulphides during the processing flowsheet.



However, the high S tailings (ENICON004), and Ni and Cu concentrates (ENICON002B and ENICON025B, respectively) do not follow the same elemental patterns, and have a much higher concentration of PGE than the ore and other tailing samples (Table 6). No PGE-sulphide has been found during this study, and their occurrence in Kevitsa has been described previously as concentrated to particular layers (González-Pérez et al., 2021), therefore it is likely that the PGE occur as trace elements within Fe-, Ni-, and Cu-sulphides. Given the modal mineralogy of the samples (described in section 3.1.5), it is possible that pyrrhotite is dictating the patterns for the high S tailings (ENICON004) and pentlandite is related to the pattern in the Ni concentrate (ENICON002B), while the highest concentrations of Pt, Pd, and Au are associated with the Cu concentrate (ENICON025B).

Given the analytical difficulty of retrieval of the Ni-pellet in the fire assay procedure for ENICON002B and ENICON025B, these results represent the minimal concentration of PGE these samples may have, and it is likely that the concentration is higher than reported here.

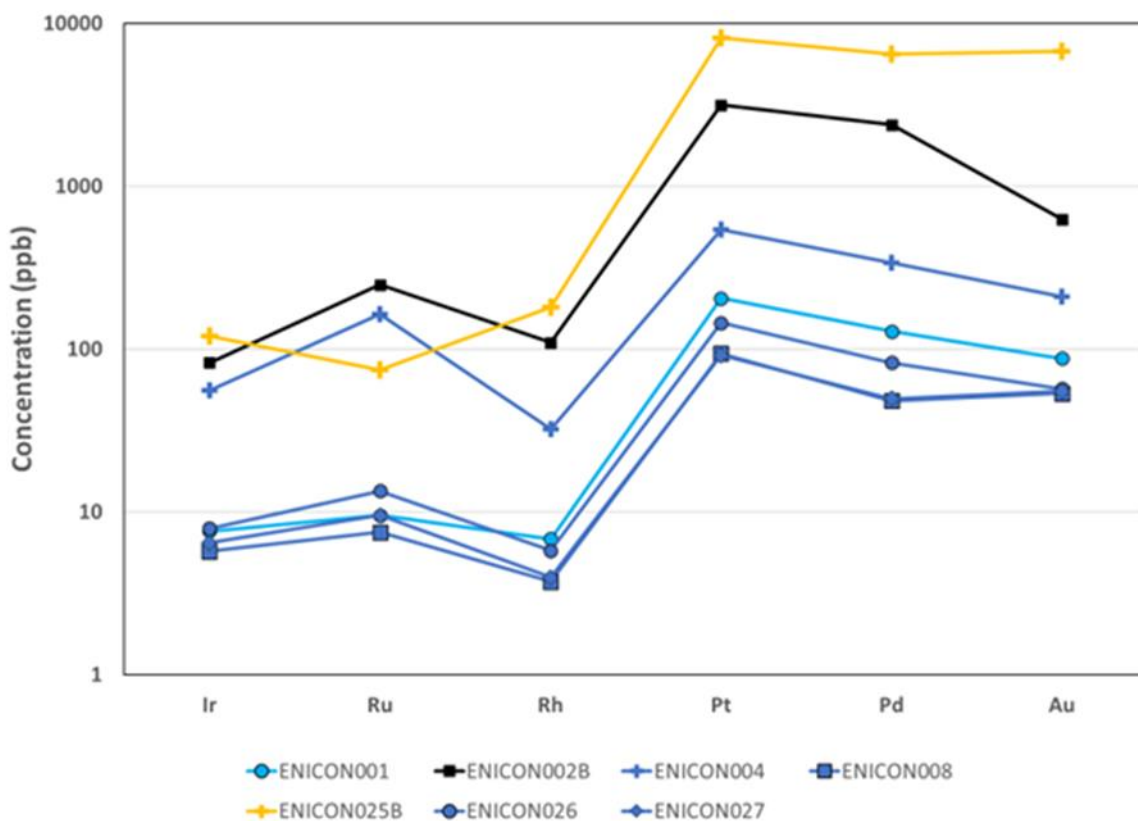


Figure 8. Pattern of platinum-group elements for the Ni/Co-sulphide samples from the Kevitsa Mine; concentration is in logarithmic scale.



Table 6. Platinum-group elements (PGE) concentrations (ppb) in samples from the processing flowsheet of the Kevitsa mine.

		Ir ppb	Ru ppb	Rh ppb	Pt ppb	Pd ppb	Au ppb
ENICON001	Ore	7.6	9.5	6.8	204.5	128.5	87.6
ENICON002B	Ni Concentrate	82.3	248.2	109.3	3153.7	2375.6	625.9
ENICON004	High S tailing	55.5	163.2	32.3	543.0	337.3	209.2
ENICON008	Low S tailing	5.7	7.5	3.7	93.7	48.1	53.4
ENICON025B	Cu Concentrate	120.2	74.5	180.1	8162.7	6479.6	6749.2
ENICON026	Cu Tailings	7.9	13.4	5.8	144.8	82.4	57.1
ENICON027	Ni Tailings	6.4	9.5	4.0	91.4	49.6	55.0

3.1.5 Modal mineralogy

The modal mineralogy of these samples was calculated by Rietveld refinement, after the XRD analyses and confirmation of the phases inferred through SEM analysis (Figure 9). The detection limit for XRD is a few wt.%, therefore minerals with low concentration are unlikely to be picked up by this method. None of the main rock-forming minerals inferred in the ore sample has Ni and/or Co as a main stoichiometric component, although we know from the literature that olivine can host significant Ni (up to 1.4 wt.%, Luolavirta et al., 2018a).

The gangue minerals in Kevitsa are amphibole, plagioclase, olivine, chlorite, serpentine, pyroxene, and calcite. Ni-minerals (pentlandite) can only be successfully quantified in the Ni-Co concentrates (ENICON002A and ENICON002B), and in those samples the remaining mineralogy is similar to the silicates and carbonates found in the ore. The Cu- concentrates (ENICON025A and ENICON025B) contain both chalcopyrite and cubanite as Cu- phases. No Co- phase has been identified in any of the samples.

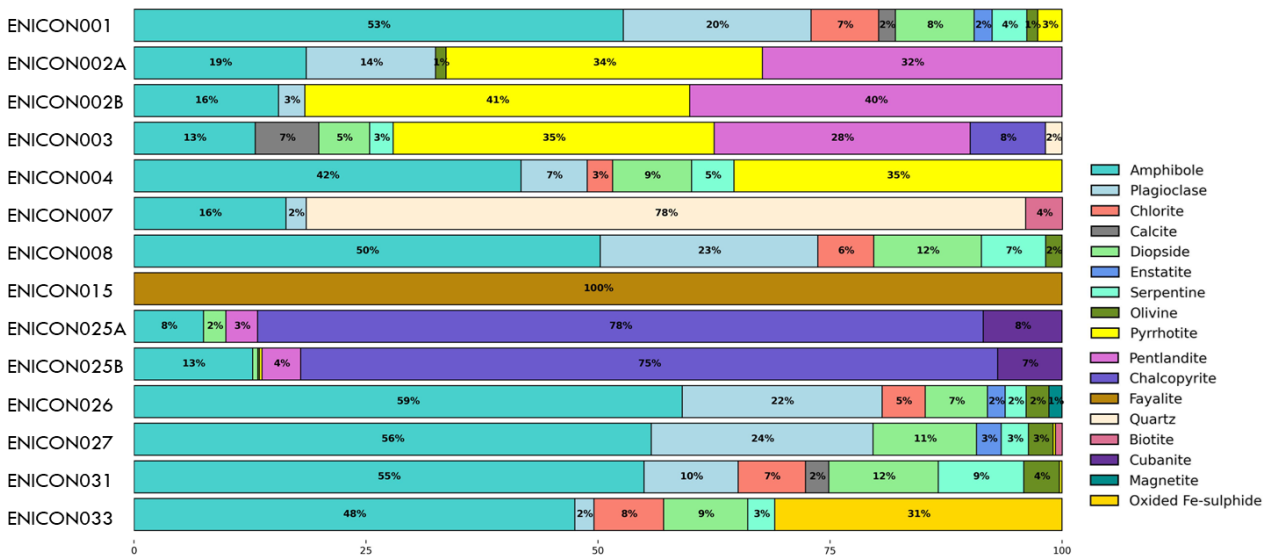


Figure 9. Modal mineralogy of the Ni/Co-sulphide samples studied in ENICON, obtained by X-ray diffraction with Rietveld refinement.

The modal mineralogy of samples ENICON033 and ENICON040 are outlined below (Figure 10). Sample 040, which corresponds to the acidic leaching of further ground sample ENICON004, has a similar modal composition to its original sample, while there is a very clear difference in the oxidative leaching sample



(ENICON033), where the Fe-sulphide is clearly oxidized. There is no change in the silicate minerals composition.

The HCl-leaching residues provided by WP2 were not analysed for XRD due to the sample size available.

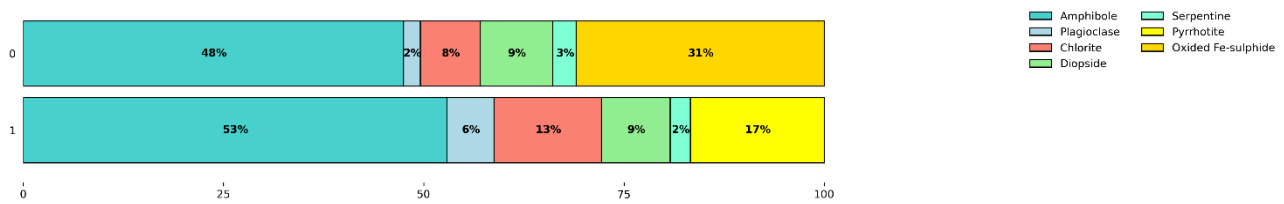


Figure 10. Modal mineralogy of the acidic and oxidative leaching residues (ENICON033, ENICON040) obtained by X-ray diffraction Rietveld refinement.

The modal analyses, when analysed in tandem with the data presented in the bulk geochemistry data (section 3.1.3), allow for comparison between the Kevitsa materials to samples from other localities. The Kevitsa Ni-Co concentrate is compared to the Ni-Co concentrate from Hautalampi (ENICON003; Figure 11). Although the Kevitsa concentrate has more pentlandite than Hautalampi (modal mineralogy estimates of 41% vs 35%, respectively), the Co content of the Hautalampi concentrate is much higher, at 2.5 wt.% (vs. 0.8 wt.% at Kevitsa, Table 3). With regards to the tailings, Kevitsa's high S tailing has more sulphides than what is observed in the historical Outokumpu oxidized pyrite tailings (up to 50% in Kevitsa, opposed to 6% in Outokumpu, ENICON007), although the pyrite tailings have a higher concentration of Co than the high S tailings (Table 4).

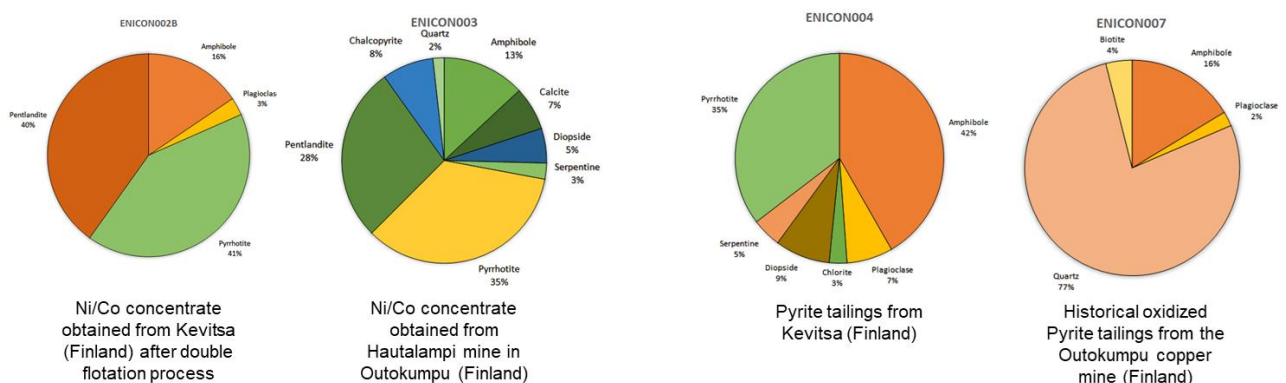


Figure 11. Pie charts of the modal composition for samples from Kevitsa and Hautalampi Ni/Co concentrates, and Kevitsa and Outokumpu tailings.

The modal mineralogy of the residues of the HCl leaching was conducted using automated mineralogy (QEMSCAN, Table 7). The main mineralogy of both samples reflects the lack of full dissolution of pentlandite (Fe-Ni sulphide) and/or formation of Ni-bearing sulphides/sulphates during the leaching stage. Although this is not possible to verify with automated mineralogy due to detection limits, it is likely that the unleached Co is also associated with these phases.



Table 7. Modal mineralogy of the HCl residues of Ni-Co concentrate and high S tailings from Kevitsa, obtained by QEMSCAN.

	Sample Name	ENICON041	ENICON042
Mineral Volume(%)	Sulphur	34.18	8.15
(Area %)	Ni Fe sulphides/sulphates	18.02	0.86
	Fe Oxides	0.24	0.18
	Chromite	0.10	0.27
	Ti minerals	0.04	0.13
	Pyrite	5.15	0.37
	Chalcopyrite	0.61	0.10
	Gypsum	4.47	0.75
	Quartz	1.95	3.61
	Plagioclase	0.36	2.88
	K-feldspar	0.06	0.18
	Chlorite	0.23	0.69
	Mg silicates	13.18	8.99
	Mg Fe silicates	6.18	10.45
	Ca Fe Al silicates	0.05	0.20
	Ca Mg (Fe) silicates	15.11	62.08
	Others	0.07	0.10

3.1.6 Mineral texture and chemistry of the sulphide ore

This section aims to look in detail at sample ENICON001, the sulphide ore from Kevitsa, in order to provide a deeper understanding of the initial material, as it has a complex mineralogy due to the blending of materials during the grinding process. The nickel bearing phase within Kevitsa is pentlandite, while chalcopyrite is the main copper phase. There is no mineral that is known to host significant amounts of cobalt. There are references in the literature about the presence of nickel within olivine (Luolavirta et al., 2018a), but relatively high concentration of nickel in olivine can only be observed in the Ni-PGE ore layers within the intrusion, reaching concentrations of up to 1.4 wt.% (Mutanen, 1997; Yang et al., 2013; Luolavirta et al., 2018a). Another Ni-bearing phase described in the literature is millerite, however, that was not observed in this study. We also have not observed any PGE-bearing sulphide, although these have been reported in this intrusion in previous studies.

Through the observation of ten thin sections cut from pieces from ENICON001 (Kevitsa stockpile), we identified two main types of rocks that were blended in the initial feed to the processing plant (Figure 12a, 12b, 12c, 12d). The first type corresponds to pristine igneous rocks, and comprises a group of rocks that has olivine, pyroxene, plagioclase, and igneous amphibole as main rock-forming minerals. We observe chalcopyrite, pyrrhotite, and pentlandite, and it is common to see these in close association with magnetite (Figure 12b, 12c, Figure 13). In these rocks, the Ni is associated with pentlandite, which can also host cobalt.

The second rock group is the metamorphic rocks, where the main rock mineralogy is amphibole (mainly tremolite) and chlorite, with minor epidote, serpentine, and biotite group minerals. In these rocks, aside from pentlandite, pyrite is also a Ni- and Co-bearing mineral (Figure 12a, 12d; Figure 13). The sulphides in these rocks are often intergrown with silicate minerals or occur disseminated (with smaller grain sizes) in the matrix of the rock. Many of the larger sulphide crystals show evidence of some alteration. Magnetite is far more abundant in these samples than in the igneous group, often being found as a “standalone” mineral, instead of being associated with sulphides.



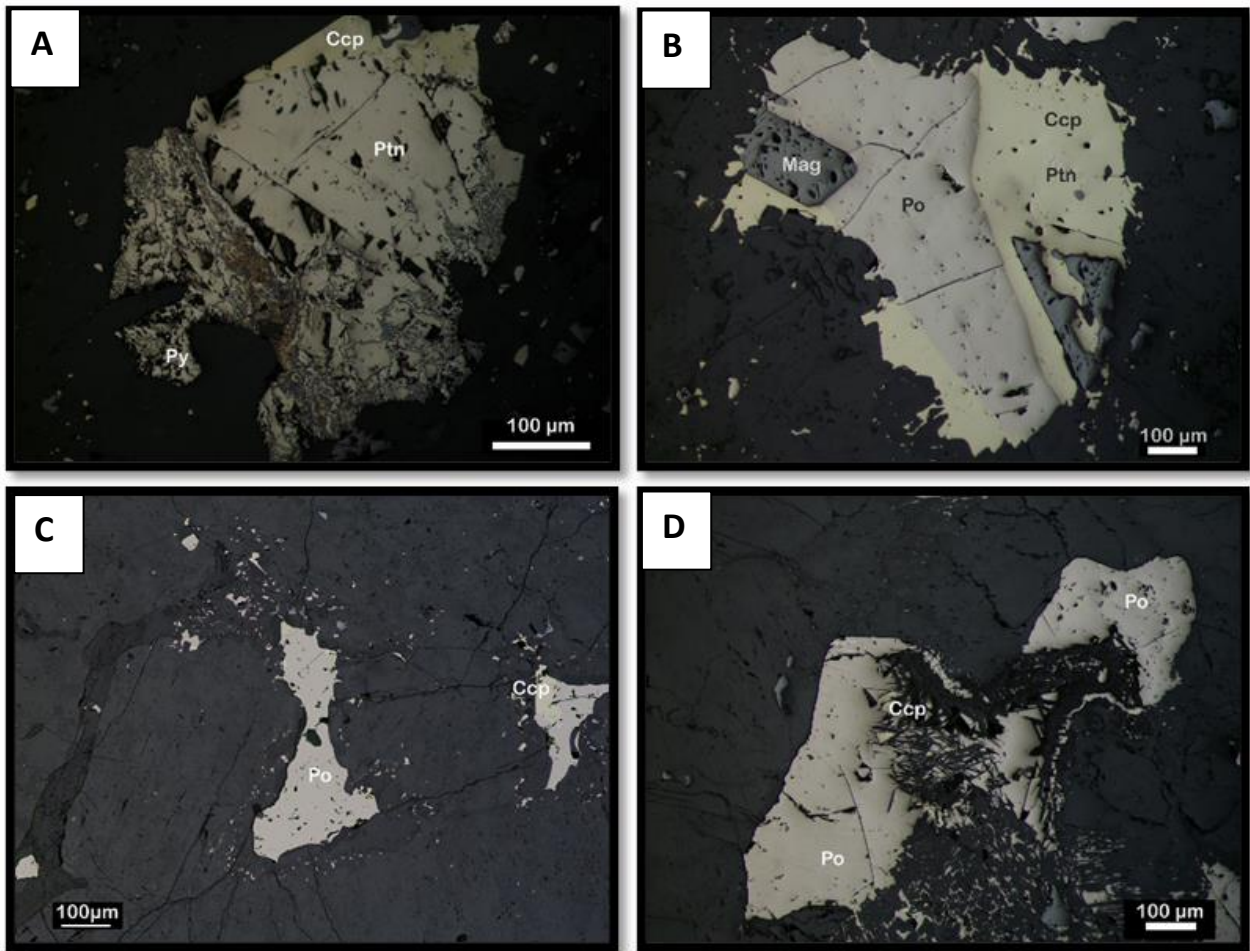


Figure 12. Reflected light optical images of sulphide ore textures. (a) Association of pentlandite (Ptn), chalcopyrite (ccp) and pyrite (py) in metamorphic rock, where pyrite occurs in altered domains of the grain; (b) association of pentlandite, chalcopyrite, pyrrhotite (po) and magnetite (mag) with an igneous texture; (c) interstitial pyrrhotite and chalcopyrite, smaller grains (<5µm) disseminated in the surrounding silicate minerals; (d) intergrowth of pyrrhotite and chalcopyrite with chlorite, metamorphic texture.

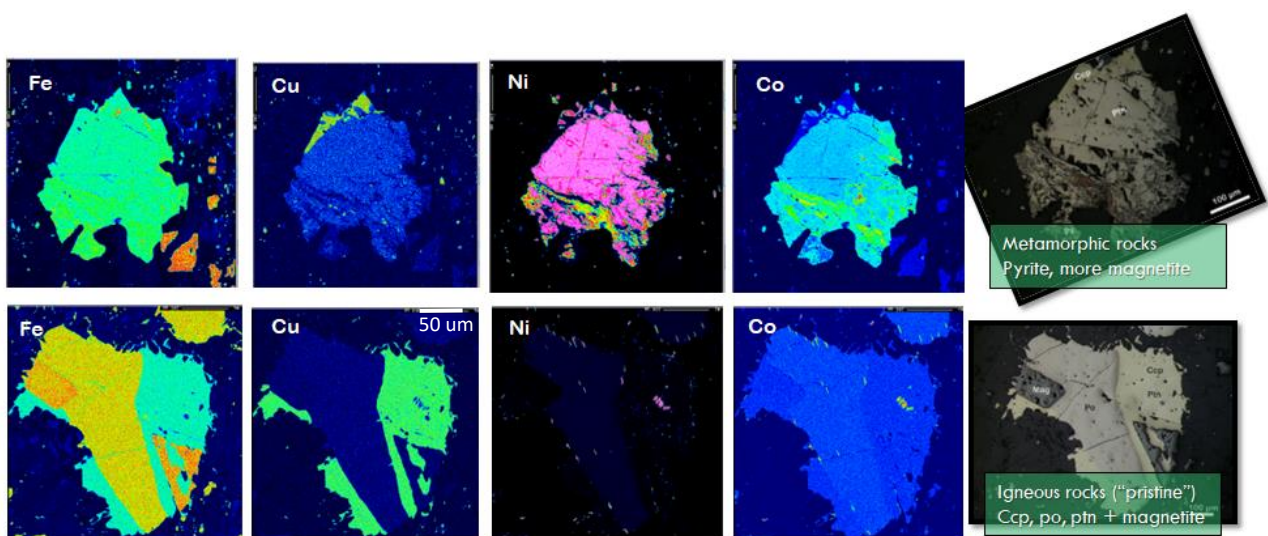


Figure 13. Qualitative WDS elemental maps of sulphide minerals from sample ENICON001, highlighting the difference in textures of the different groups of rocks found in this blended material. Warmer colours (white as the maximum value) reflect higher elemental concentrations and cooler shades (black as the minimum value) correspond to lower amounts.



We measured the NiO (wt.%) content in both silicate and oxide minerals (Figure 14), and as Ni metal in sulphides. The main Ni-bearing phase is pentlandite, as expected. However, significant Ni has also been measured in pyrite, chromite, and magnetite (up to 2.39 wt.%, 0.3 wt.%, 0.25 wt.% respectively). The content of Ni in olivine can also reach up to 0.25 wt.%, however, it is highly variable within crystals from the same sample as well as between different samples (Figure 15). A compilation of available literature data (Yang et al., 2013; Luolavirta et al., 2018a; Luolavirta et al., 2018b, Figure 16) shows the high variability of the Ni content in olivine within the Kevitsa intrusion, which reaches up to 1.8 wt.% NiO, although such value has not been observed in our study.

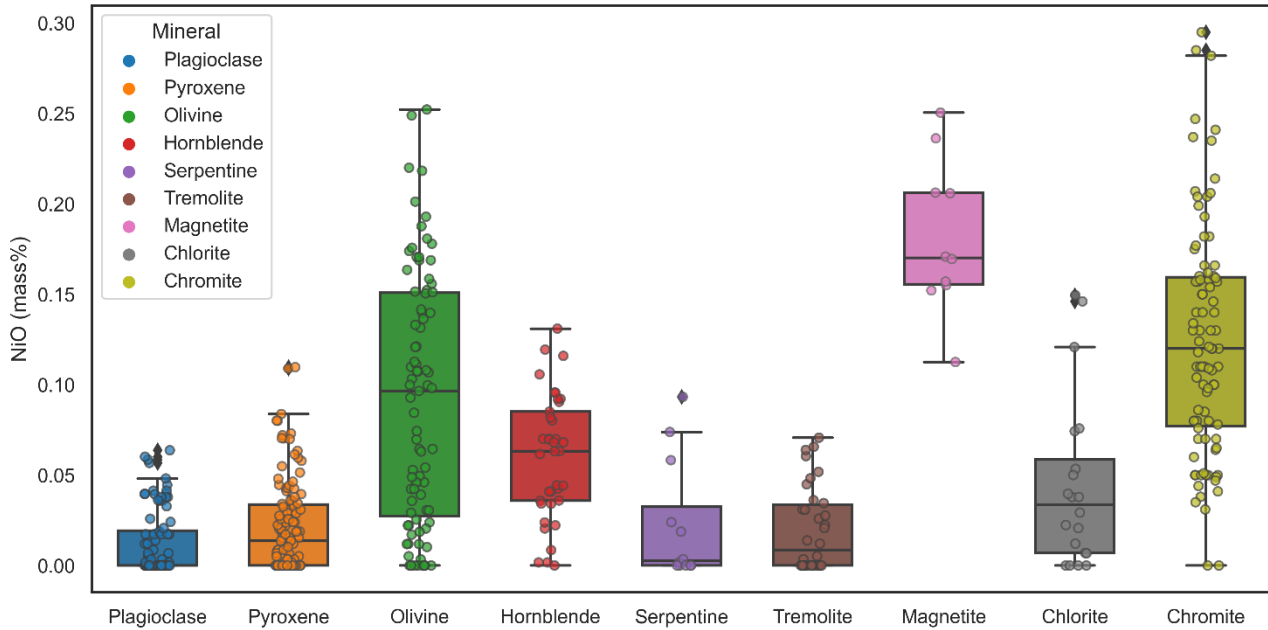


Figure 14. NiO concentration (mass%) in the main minerals of the rocks that combined represent the sulphidic ore (ENICON001). Chromite data obtained from literature (Luolavirta et al., 2018b; Gonzalez-Perez et al., 2021)

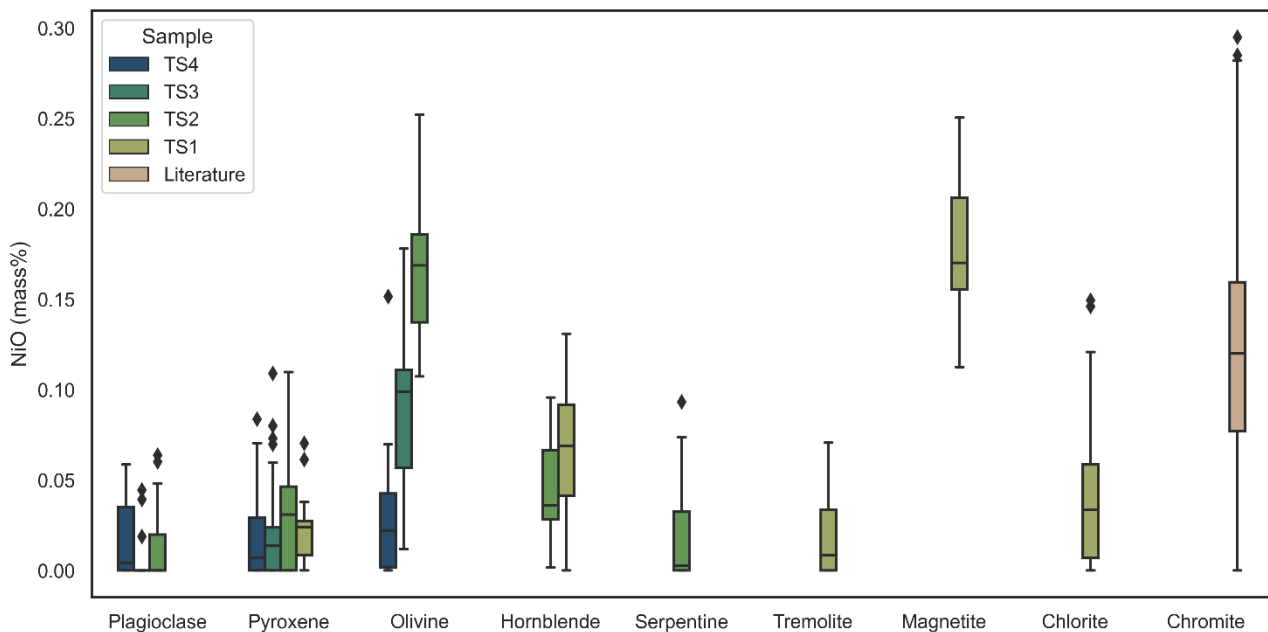


Figure 15. Variation of NiO (mass%) within different thin sections of ENICON001, showing intra-sample compositional variation in the NiO concentration within olivine.



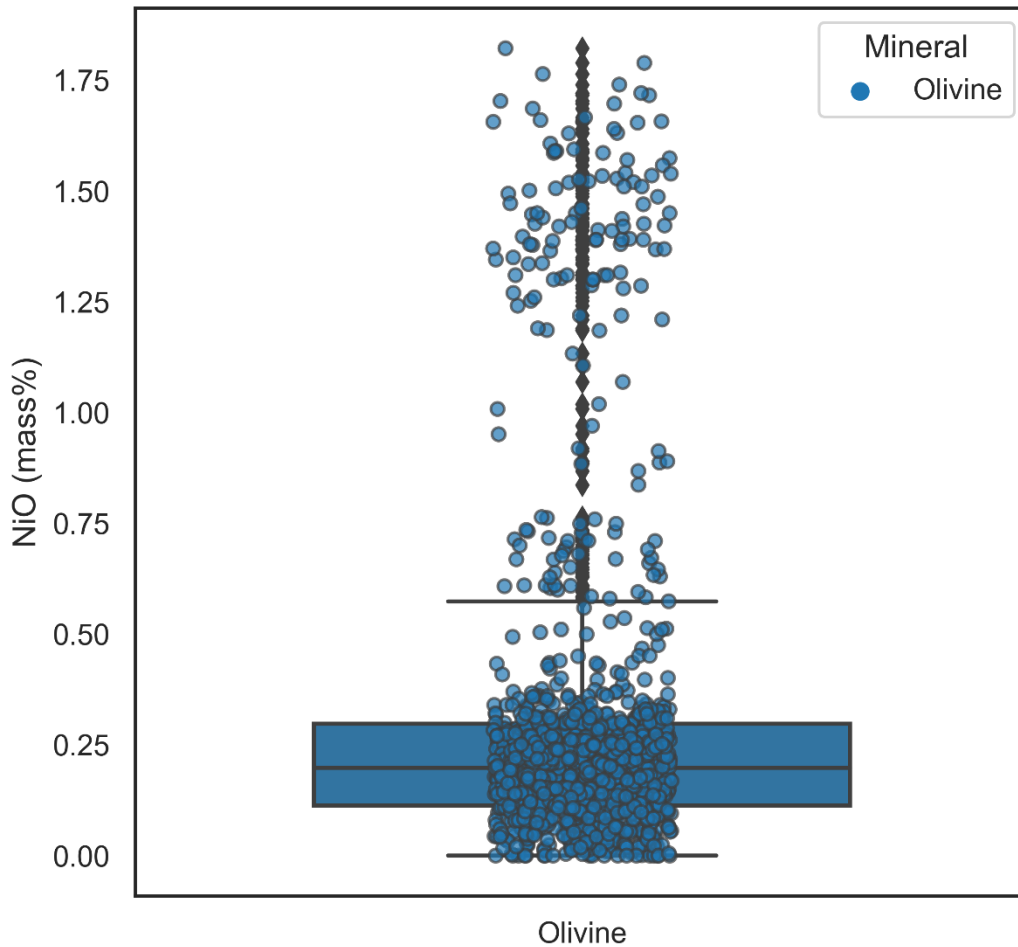


Figure 16. Compilation of literature data available on the olivine composition of the Kevitsa Igneous Complex (Yang et al., 2013; Luolavirta et al., 2018a; Luolavirta et al., 2018b, this report).

For cobalt, however, we do not see the same behaviour. While pentlandite is also the mineral that hosts the higher contents of Co within the Kevitsa rocks (up to approximately 1.4 wt.%), pyrite can also host significant cobalt (up to 2.3 wt.%). It is worth noting that EDS data obtained in the Kevitsa tailings suggest that the concentration of cobalt can be higher in pentlandite, although we have not been able to observe this in the rocks from ENICON001.

Magnetite and chromite are Co-bearing, and can reach concentrations of up to 0.2 wt.% CoO. Most silicate minerals have negligible cobalt content, and the maximum CoO concentration measured in olivine is 0.12 wt.% (Figure 17).

While we saw variability in the nickel content within olivine, the same is not seen for cobalt, which suggests a decoupled behaviour between the two elements (figures 15 and 18).



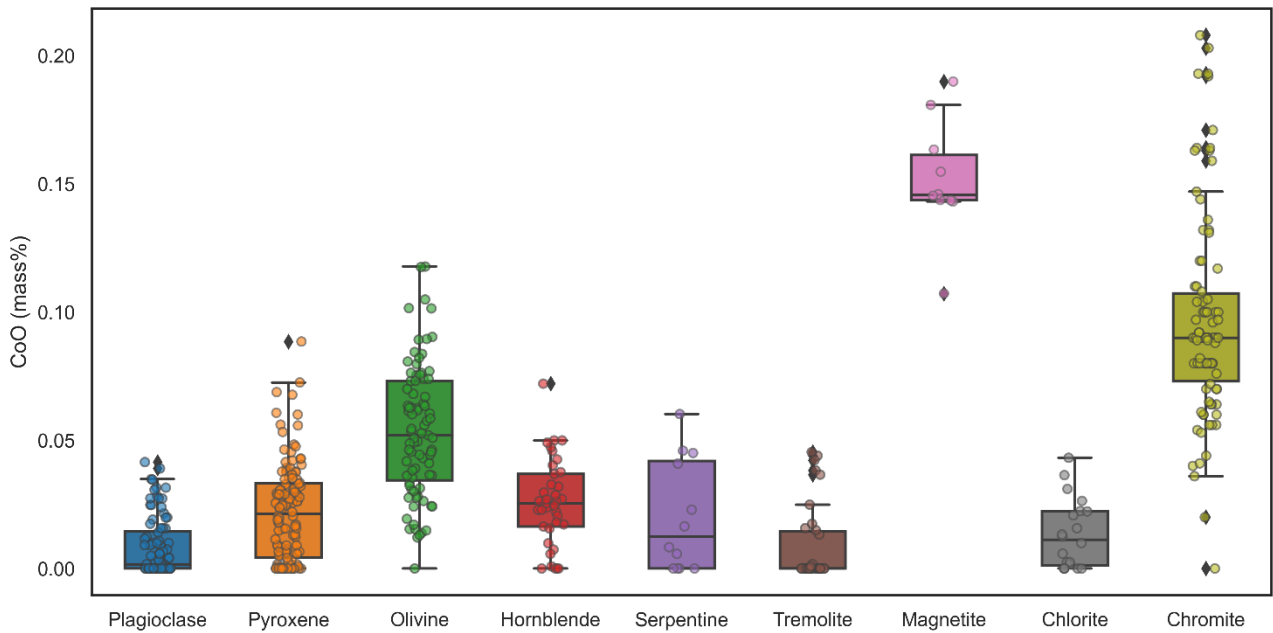


Figure 17. CoO concentration (mass%) in the main minerals of the rocks that combined represent the sulphidic ore (ENICON001). Chromite data obtained from literature (Luolavirta et al., 2018b; Gonzalez-Perez et al., 2021)

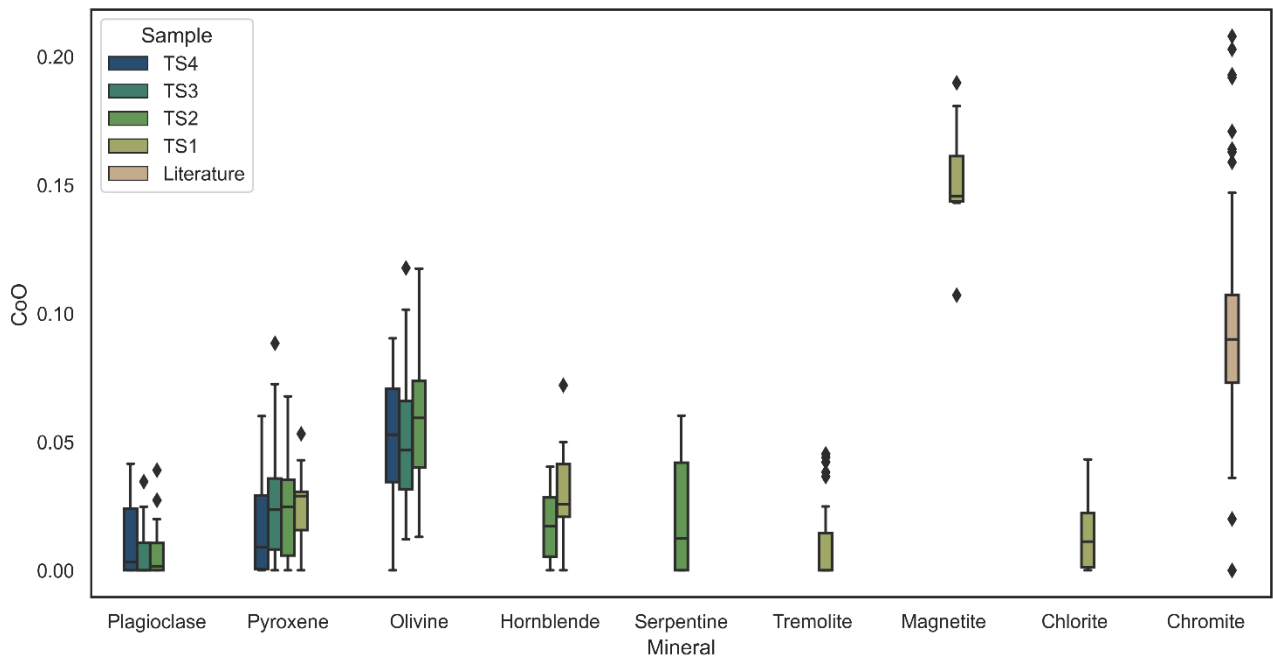


Figure 18. Variation of CoO (mass%) within different thin sections of ENICON001, showing that there is no variation in the concentration of cobalt between different blended materials.

3.1.7 Surface chemistry (XPS)

Two samples were studied using XPS, ENICON025A (Cu concentrate) and ENICON033 (leaching residue). Other ENICON samples were studied, however due to a server issue, data was not saved properly, requiring a new analytical run, yet to be conducted.



The survey of the Cu concentrate (ENICON025A, Figure 19) reveals the chemical composition of the sample's surface. Oxygen constitutes the majority at approximately 38%, which is unsurprising given the sample's composition of mixed minerals. Carbon follows with an atomic percentage of 22%.

The sample contains various silicates, which is reflected by the 18.4% Si at the surface. Sulfur is present at a concentration of 14%, reflecting the presence of sulphides. Iron is detected at 4%, while Cu makes up 1.3%. Trace amounts of other minerals are also present.

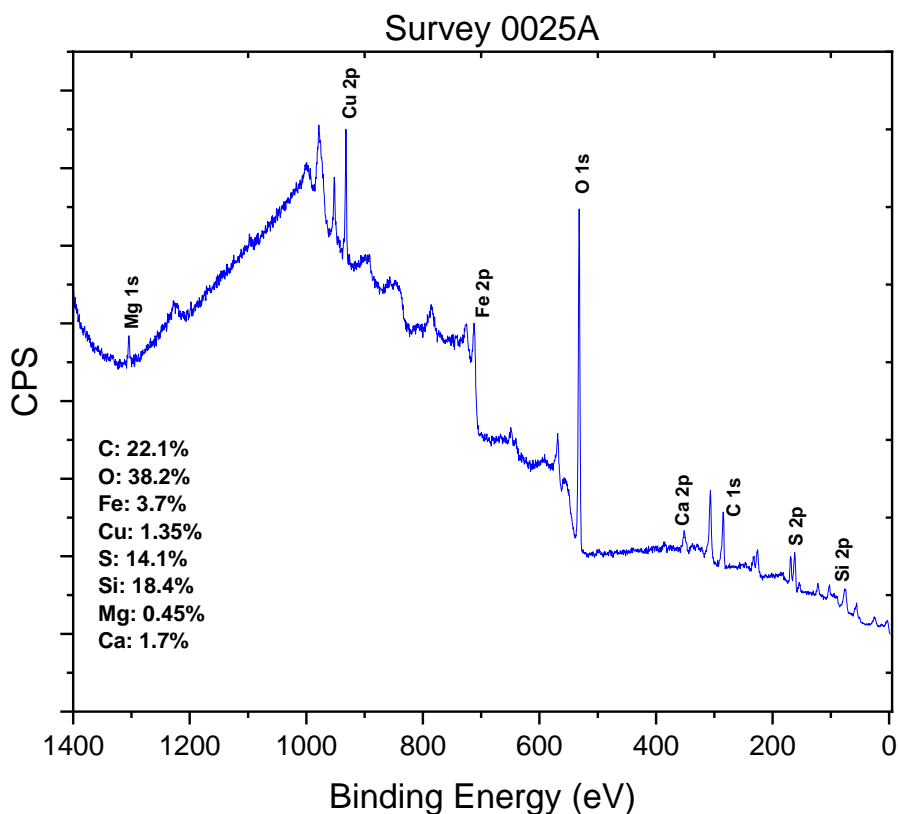


Figure 19. XPS spectra of sample ENICON025A, showing the peaks for different elements.

The sample contains two iron species: Iron(III), which is the majority (~87%), and Iron(II) (~13%), in an approximate ratio of 7:1. The fitting was performed by superimposing data from Fe(II) and Fe(III) standards (Figure 20).

Sulphur was initially fitted with three components: sulphide (161.3 eV), disulfide (163.3 eV), and sulphate (168.8 eV) – Figure 20. A fourth component near 166 eV is under consideration, though additional evidence is required to confirm the presence of more sulphur species.

Silicon plasmons were ruled out after analyzing the Si 2p and Si 2s regions. The atomic concentration ratio for sulfur species is approximately 4:1:2.5 (sulfide:disulfide:sulfate).

Additional data collection is necessary. Preliminary findings suggest the presence of copper in a mixed oxidation state (Cu(I) and Cu(II)), with Cu(I) being the dominant form.



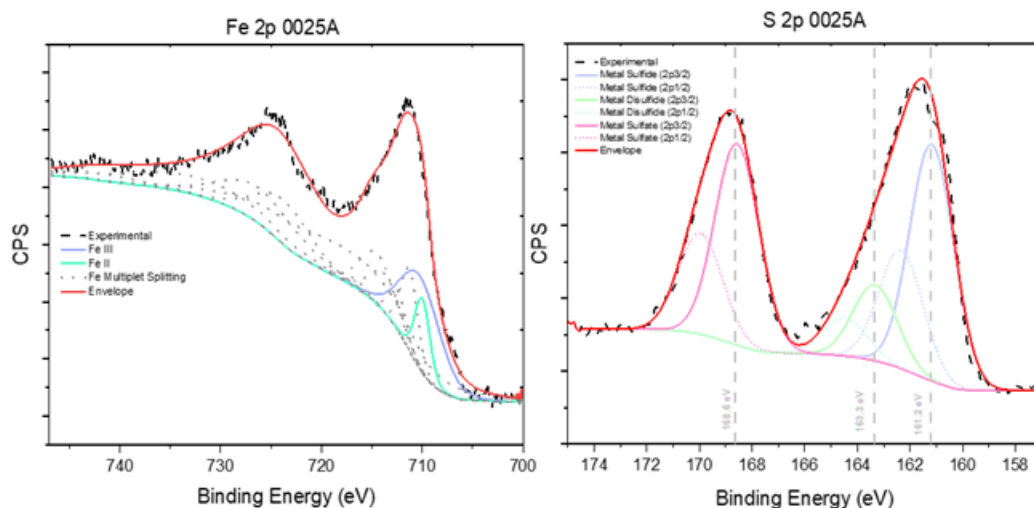


Figure 20. High-resolution XPS peak fits for iron (left) and sulphur (right) in sample ENICON025A, allowing for the discrimination of the different species of each element.

Like sample ENICON025A, sample ENICON033 primarily consists of oxygen (55%), followed by silicon (~18%) and carbon (~13%). No copper was detected on the sample's surface (Figure 21). Sulphur is present at approximately 9%, while iron accounts for 3%. Trace amounts of other elements were also identified.

High-resolution analysis of iron and sulphur (Figure 22) reveals a notable difference from the previous sample. Iron is present in both iron(II) and iron(III) states, with a ratio close to 1:4 (II:III). Sulphur exists in two distinct chemical environments: metal disulphide and sulphate, with a ratio of 1:8 (disulphide:sulphate). This ratio may correlate with the iron composition, explaining the chemical differences compared to sample ENICON025A. Additionally, the absence of sulphide components aligns with the higher proportion of iron(III) relative to the earlier sample.



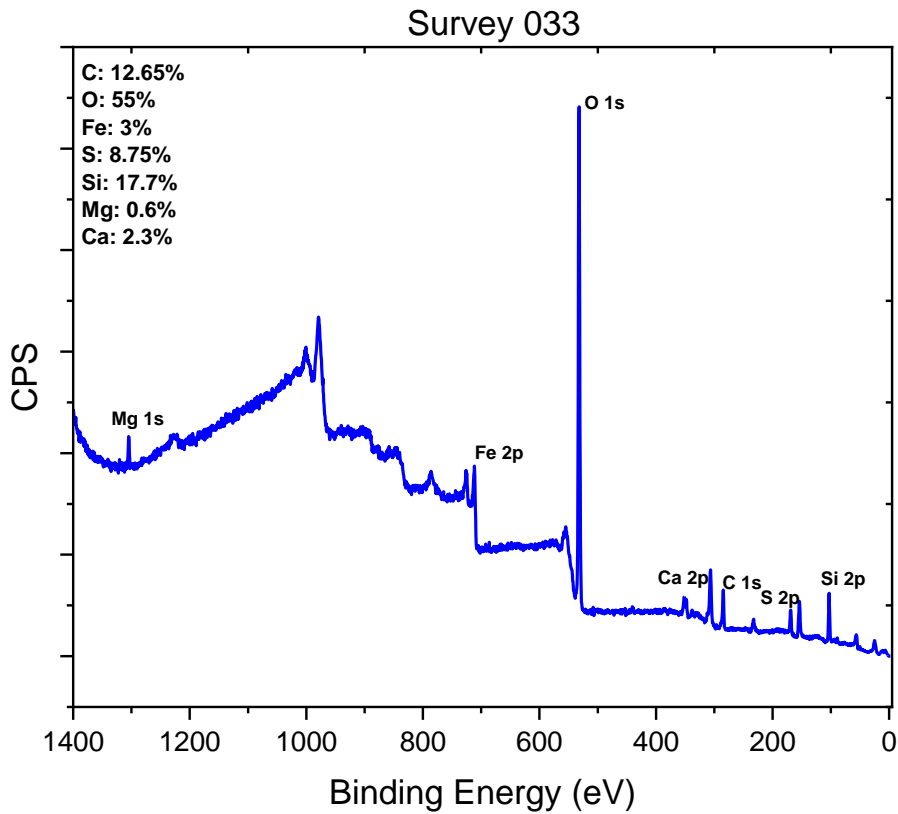


Figure 21. XPS spectra of sample ENICON033, showing the peaks for different elements.

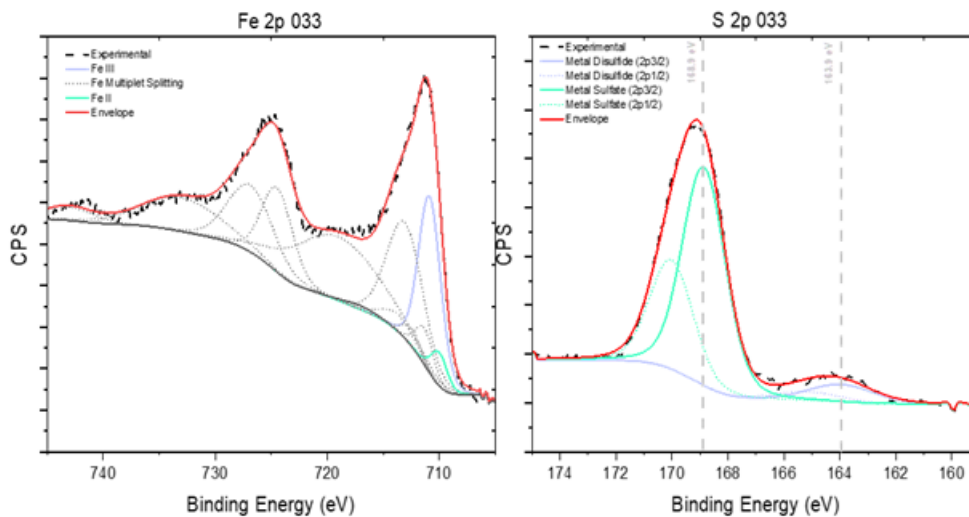


Figure 22. High-resolution XPS peak fits for iron (left) and sulphur (right) in sample ENICON033, allowing for the discrimination of the different species of each element.



3.1.8 Sequential extraction

Sequential extraction was conducted for three tailings samples, Kevitsa's high and low sulphur tailings and Outokumpu's pyrite tailings (respectively, ENICON004, ENICON008, and ENICON007), to assess the potential for chemical mobilization of metals, as metal leachates from mine tailings have the potential to release toxic metals into the surrounding environment. The three-step BCR sequential extraction mimics slightly acidic (step 1), reducing (step 2), and oxidizing (step 3) conditions.

The three samples exhibit different leaching profiles for the elements studied except for V and Sc, which are highly concentrated in the residual fraction in all three samples (i.e. it is mostly not being leached in any of the experimental conditions). The analysis of the high S tailings (ENICON004, Figure 23) showed that under acidic conditions, about 20% of the Zn was released, along with lesser amounts of Cu and Pb. Under reducing conditions Pb was the main element being leached along with some Zn. Oxidizing conditions are the most favourable for the leaching of Ni, Co and Cu, along with some Pb, Zn, and As. Over 50% of the Ni, Co, Cu, and As remain in the residue, as well as 40% of Pb and Zn.

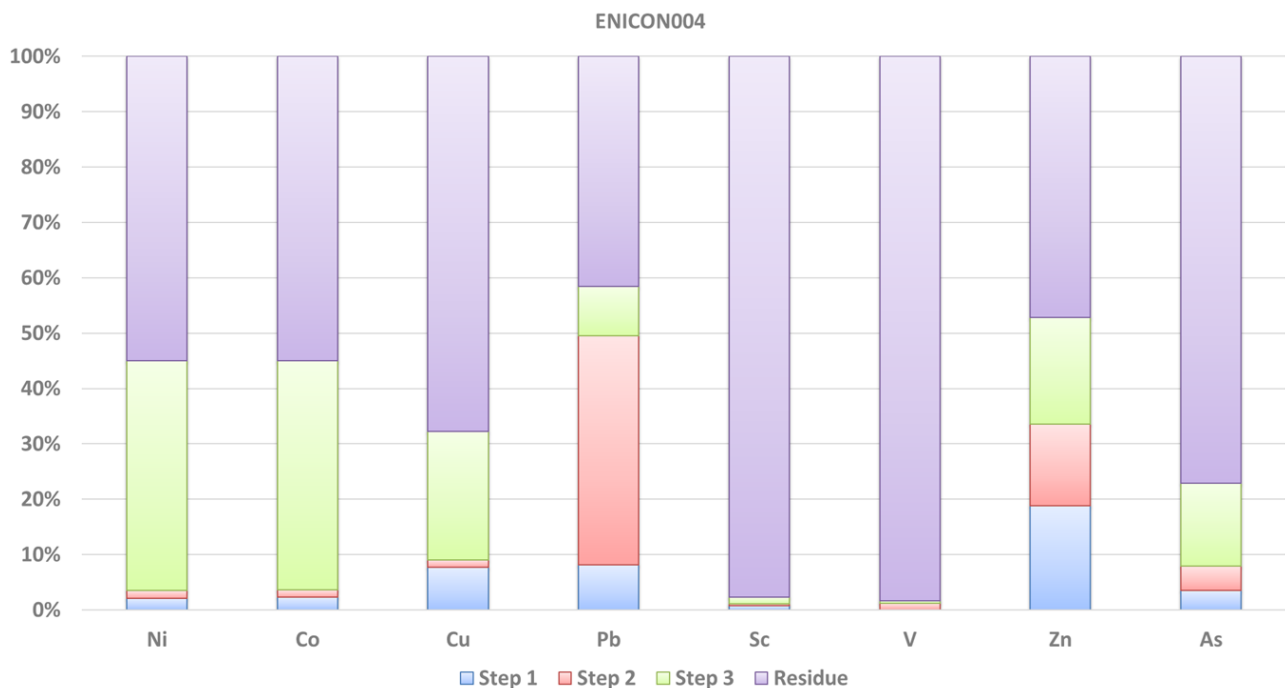


Figure 23. Sequential extraction data for sample ENICON004 for a selection of elements.

The results from the low S tailings (ENICON008, Figure 24) show a different leaching profile. While Sc and V remain mostly in the residue as in the previous sample, approximately 10% of Ni, Co, Cu, Pb, As and 20% of the Zn are leached under acidic conditions. Under reducing conditions, 20% of the Pb and nearly 10% of the Zn and As are leached. In oxidizing conditions, a significant percentage of Ni, Co and Cu are leached (approximately 45%, 30%, and 55%). 60% of the Zn, 75% of the As, 55% of the Co, and 50% of the Pb remain in the residue.



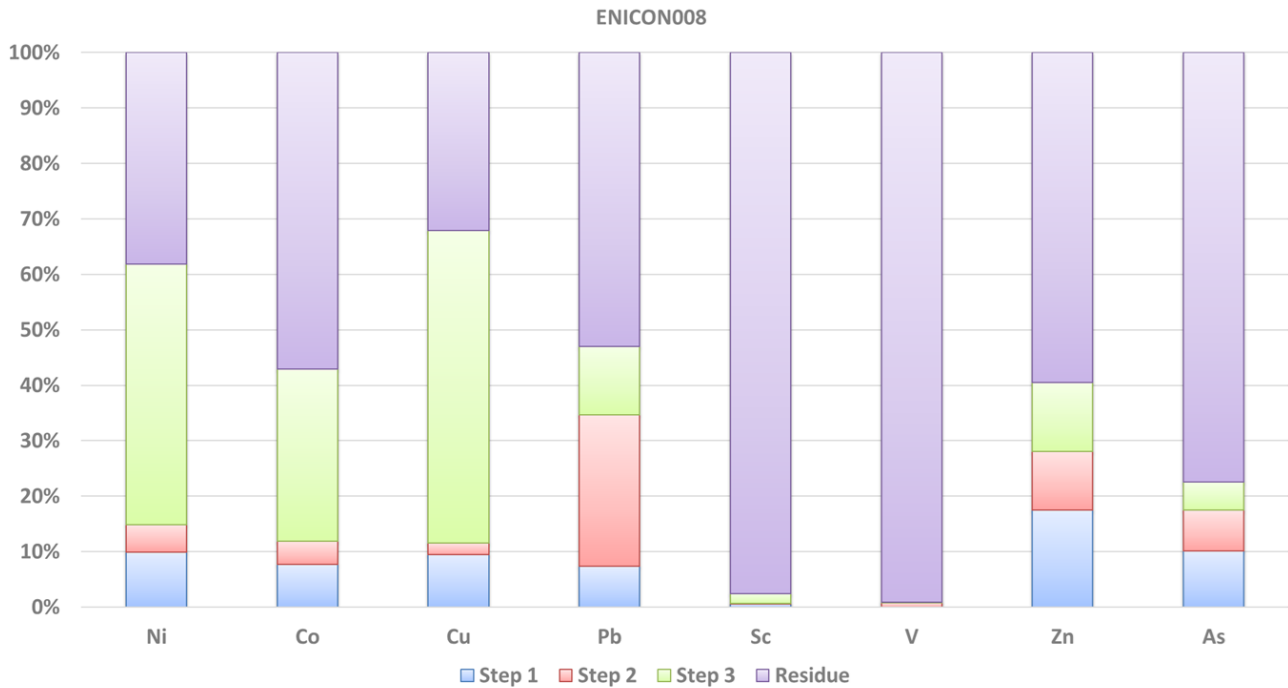


Figure 24. Sequential extraction data for sample ENICON008 for a selection of elements.

The historical oxidized tailings from Outokumpu show yet a different profile (Figure 25). In this case, aside from most of the Sc and V remaining in the residue, As is also mostly retained. Ni, Co, Cu, and Zn are extractable in both acidic and oxidized conditions, while Pb is extracted in reducing conditions.

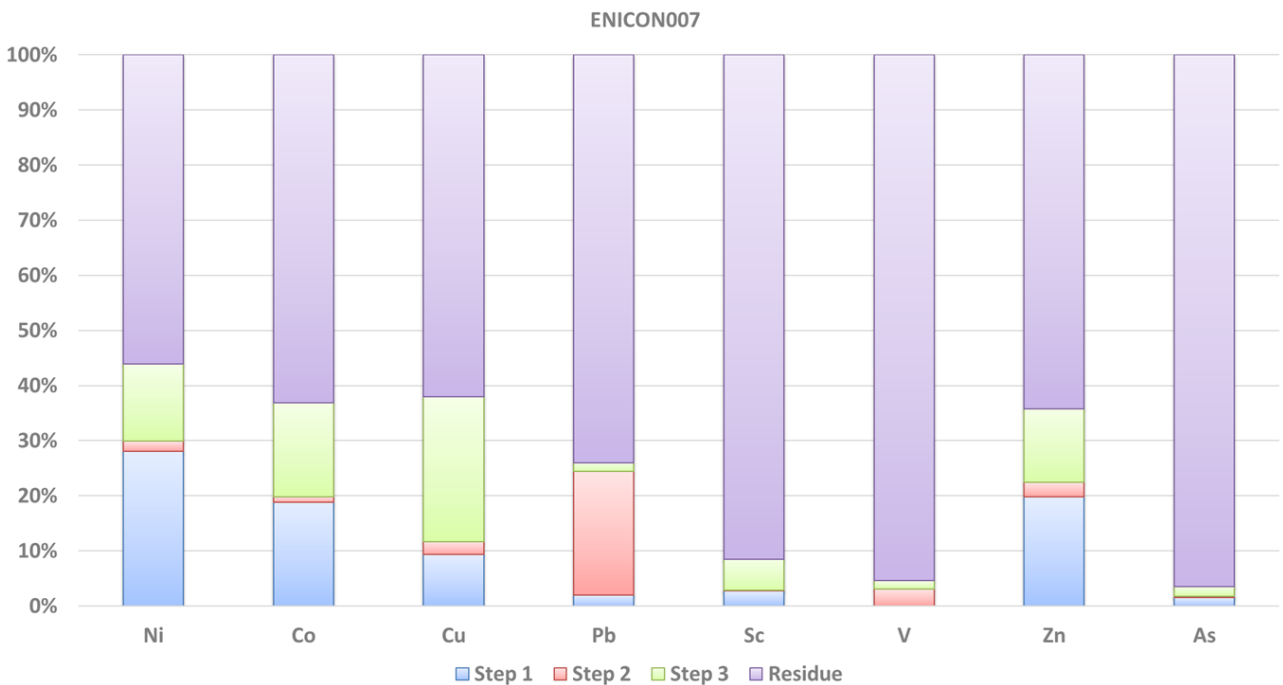


Figure 25. Sequential extraction data for sample ENICON007 for a selection of elements.

The difference in leaching profiles between different samples might reflect the sulphide mineralogy of the samples, either due to separate phases hosting a certain element (e.g., different Pb-bearing sulphides), or different proportions of the same sulphide



3.1.9 Metal department and mass balance

The metal department of the sulphidic ore (ENICON001) can be seen in Figure 26. The nickel department can be divided in several different minerals, the most important being pentlandite (~62%), with a significant contribution from olivine (~25%). Minerals that contribute to it in a smaller proportion are magnetite, pyrite, chromite, and pyrrhotite (each less than 5%). The main host of cobalt in the ore is pyrite, which holds approximately 50% of the cobalt budget. Olivine is also a big contributor (ca. 28%), followed by magnetite (10%), pentlandite (10%), and chromite (2%). Chalcopyrite corresponds to the whole budget of copper.

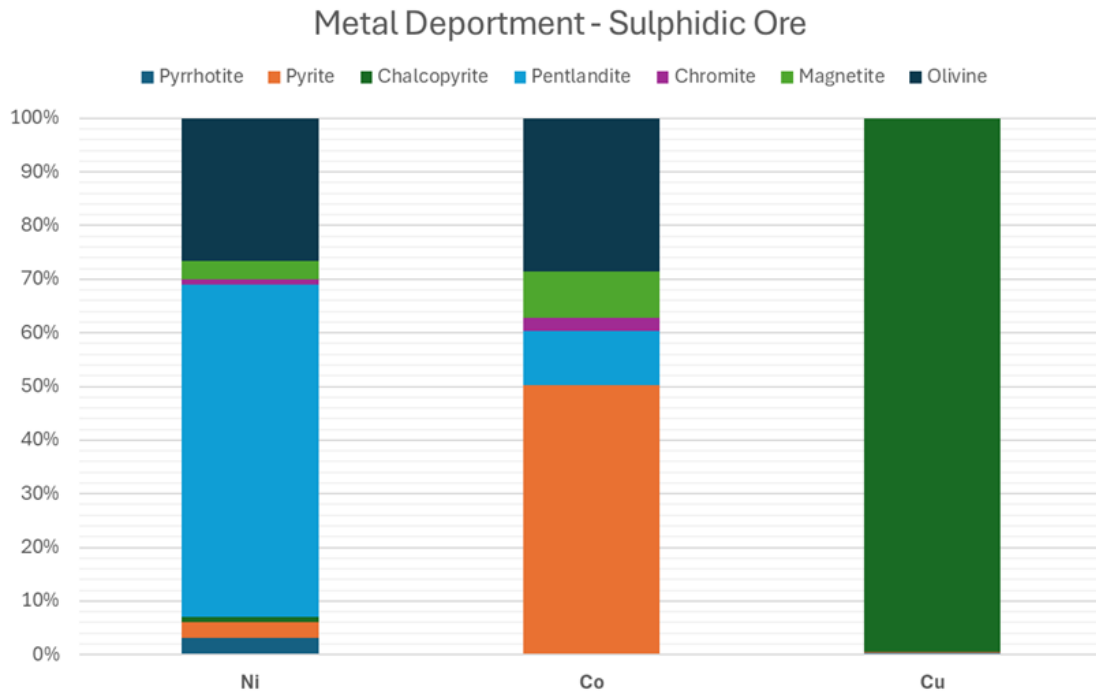


Figure 26. Department of Ni, Co, and Cu in the sulphidic ore from Kevitsa (ENICON001).

Once the flowsheet process of Kevitsa reaches the concentrate stage (ENICON002B), the department of metals changes drastically (Figure 27) due to the change in mineral proportion in the material; pentlandite hosts almost 100% of the nickel and 90% of the cobalt (the remaining 10% is hosted in pyrite). Chalcopyrite remains the main source of copper.



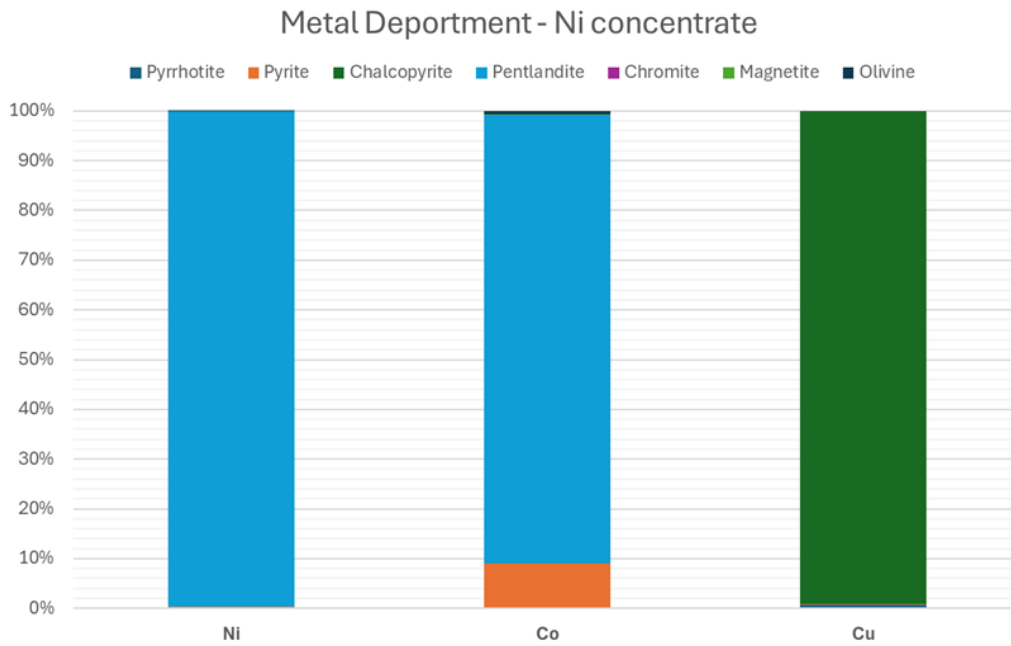


Figure 27. Department of Ni, Co, and Cu in the Ni concentrate (ENICON002B) of the sulphidic flowsheet.

The nickel (>9000 ppm, Table 5) in the high S tailings (ENICON004) is hosted predominantly in pentlandite, with a small contribution from pyrrhotite and pyrite. This sample contains approximately 434 ppm of Co (Table 5), which is largely hosted in pentlandite, although there are significant (ca. 10%) contributions from olivine, 7% from pyrite, and 4% from magnetite. Again, the budget of Cu is entirely hosted in chalcopyrite (Figure 28).

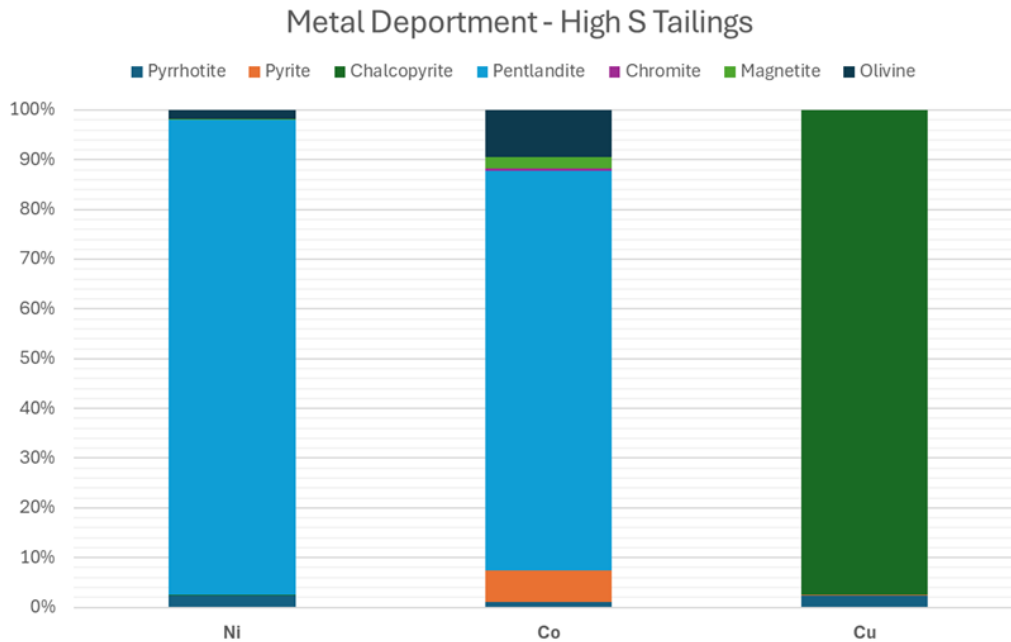


Figure 28. Department of Ni, Co, and Cu in the high S tailings (ENICON004) of the sulphidic flowsheet.

It is not possible to determine the department of arsenic as it has a low concentration in the whole rock, and therefore, its concentration in minerals was below the detection limit in the EPMA.

It was not possible to calculate the mass balance between the Kevitsa materials and leaching routes due to the unavailability of critical data at the present moment.



3.2 Task 1.2 – Ni/Co laterite ores

Chemical, mineralogical and textural characterization of laterite ores and gangue, solid products from the original smelting process and leaching residues from WP2; Analyses of main and trace elements of mineral phases within those samples; mass-balance calculation and flowsheet analysis for metal department in laterite ores & derived materials in WP2.

3.2.1 Investigated flowsheet and sample information

Three leaching tests are investigated in this report. Although all of them follow a similar flowsheet (Figure), their conditions varied slightly in the leaching stage.

The first test corresponds to leaching the laterite ores after crushing them below 0.5 mm, producing residues ENICON034, ENICON035, ENICON036, and ENICON037. This leaching test was carried out using a small-scale lab setup with HCl 8 mol/L (acid concentration), 100 to 200 g/L (S/L, solid-to-liquid ratio), stirring at 400 rpm for 3 hours at 95 °C. These residues are the main references to compare the efficiency of the process between all samples.

The second test was carried out only with laterite ores ENICON016 and ENICON020, producing residues ENICON038 and ENICON039. This test used the same conditions as the previous but with the addition of an oxidizing agent (H₂O₂) during leaching. The amount of residue obtained in sample 039 was not enough to carry out all the measurements in the protocol, with only mineralogical data further reported.

The last test was carried out on laterite ores ENICON017 and ENICON028. This time, the input material was the ROM sample (not crushed), producing residues ENICON043 and ENICON044. The leaching conditions used are similar to the first test with the crushed material 8 mol/L HCl, S/L = 200 g/L, 8 hours, 80 °C, 200 rpm.

In all cases, after filtration of the pregnant leaching solution (PLS) containing the dissolved metals, the retained solid residues were washed with distilled water to remove any excess acid before following the same processing workflow as ore samples (e.g., splitting and milling) towards characterisation.

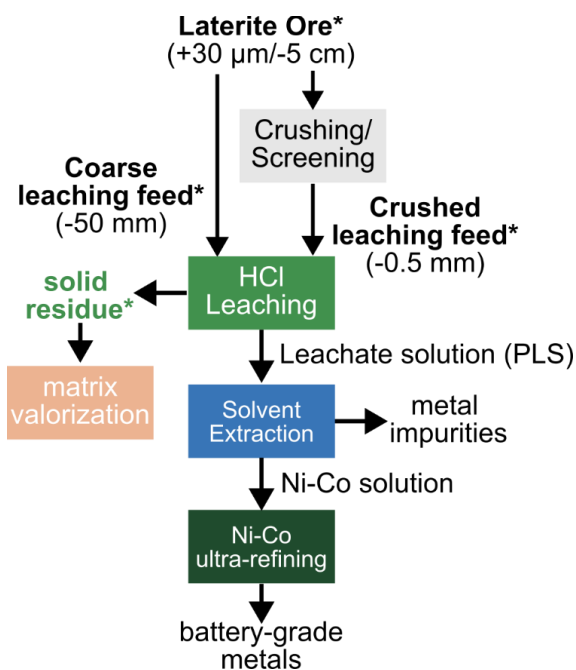


Figure 29: Simplified flowsheet representation with the input and output streams investigated in WP1 of the ENICON project. The samples used in this study are in bold and marked with an asterisk.



3.2.2 Whole-rock geochemistry

The laterite ores (ENICON016, ENICON017, ENICON020, and ENICON028) are rich in SiO₂, Fe₂O₃, Al₂O₃, and MgO, with CaO also important in some cases (Figure 30 and Table 8). Bulk nickel content varies from around 1 to 2 mass%, whereas the cobalt content ranges from 250 to 1000 ppm (Table 9).

Compared to the ores, the leaching residues are enriched in SiO₂ and CrO₂ (Figure), with similar concentrations of Co, Zn, and V (Table 9). The Ni concentration in all leaching residues is several orders of magnitude lower than in the ores, whereas Co mostly shows similar ranges between ores and residues. The exception is sample ENICON028, i.e. the sample with the highest grade, where the Co concentration of the residue is significantly lower than in the ore.

Comparing the different leaching tests, the solid residues do not show significant differences in their compositions, with the main variations related to the input materials (Figure). However, the residues from the coarse feed (ENICON043 and 044) contain more Ni and Co than the residues after leaching the crushed samples (ENICON035 and 037). This difference (Figure 3) is more evident for the limonitic laterite (ENICON017 -> ENICON035 vs ENICON043).

The loss on ignition (LOI) of leaching residues was not measured due to the low amount of material available. Negative LOI (i.e., gain on ignition) in the slag samples is due to oxidation, likely of iron, at high temperatures (Vandenberghe et al., 2010).

Table 8: Bulk major element composition (oxide mass%) of laterite ores and leaching residues investigated in this study. *Data for FeNi granules (ENICON023 and 024) are in elemental mass%.

Sample	SiO ₂	TiO ₂	Al ₂ O ₃	Cr ₂ O ₃	Fe ₂ O ₃	MnO	MgO	CaO	Na ₂ O	K ₂ O	P ₂ O ₅	NiO	CoO	LOI	Total (%)
ENICON016	37.0	0.02	1.0	1.2	22.1	0.3	15.1	8.2	0.02	0.04	0.02	1.3	0.04	14.6	101.1
ENICON017	36.1	0.3	6.5	2.2	38.9	0.2	4.8	2.2	0.06	1.1	0.01	1.2	0.06	4.9	100.3
ENICON020	14.6	0.2	5.5	1.9	53.9	0.5	3.0	4.4	0.04	0.1	0.05	1.2	0.06	10.8	97.0
ENICON028	36.4	0.06	4.2	1.3	32.0	1.0	5.9	3.4	0.02	0.06	0.02	2.8	0.14	15.0	100.8
ENICON021	38.9	0.41	9.2	2.3	38.8	0.3	7.2	5.2	0.00	0.5	0.04	0.1	0.01	-3.7	99.2
ENICON022	44.0	0.14	4.8	1.7	27.6	0.5	19.7	3.4	0.00	0.16	0.03	0.1	0.01	-2.5	99.7
ENICON023*	< 0.01	< 0.01	< 0.01	< 0.01	78.1	< 0.01	0.04	0.03	< 0.01	< 0.01	0.04	21.7	1.00	n.a.	100.9
ENICON024*	< 0.01	< 0.01	< 0.01	< 0.01	77.5	< 0.01	0.03	< 0.01	< 0.01	< 0.01	0.03	24.2	0.62	n.a.	102.5
ENICON034	83.0	0.03	0.8	2.1	1.0	0.1	1.2	0.2	0.04	0.05	< 0.01	0.02	0.02	n.a.	88.6
ENICON035	79.9	0.2	4.2	4.3	3.2	0.1	1.6	0.1	0.1	0.9	< 0.01	0.1	0.02	n.a.	94.6
ENICON036	68.7	0.3	6.0	5.9	2.8	0.3	1.9	0.2	0.2	0.3	0.01	0.1	0.07	n.a.	86.9
ENICON037	84.0	0.06	2.2	1.8	1.4	0.02	0.7	0.1	0.02	0.02	< 0.01	0.05	0.003	n.a.	90.4
ENICON038	84.2	0.03	0.8	1.8	0.8	0.1	1.1	0.4	0.05	0.1	< 0.01	0.01	0.02	n.a.	89.3
ENICON043	72.6	0.3	5.8	4.4	7.2	0.1	2.3	< 0.01	0.1	1.3	0.01	0.2	0.02	n.a.	94.5
ENICON044	70.9	0.1	2.3	1.7	2.0	< 0.01	0.6	< 0.01	< 0.01	< 0.01	< 0.01	0.08	0.004	n.a.	77.7

LOI = loss on ignition; n.a. = not analyzed



Table 9: Minor and trace element concentrations (ppm) of elements of interest in laterite ores and leaching residues

Sample	Ni	Co	S	Zn	V	Cu	Sc	Pb	As
ENICON016	10113	292	116	152	80	21	18	2.2	1.0
ENICON017	9290	452	529	180	176	33	34	8.2	8.2
ENICON020	9646	509	200	262	224	64	51	6.7	6.0
ENICON028	21724	1069	273	274	119	47	62	bdl	815
ENICON021	988	89	1129	71	238	17	44	2.9	4.5
ENICON022	1037	64	458	190	165	37	32	4.9	2.6
ENICON023	216552	9952	722	bdl	7	707	bdl	18	931
ENICON024	241810	6221	2488	bdl	6	429	bdl	13	75
ENICON034	150	145	bdl	141	89	4.0	1.5	bdl	bdl
ENICON035	809	136	512	377	180	8.4	12.2	bdl	1.6
ENICON036	1206	574	37	733	244	8.6	4.0	bdl	2.2
ENICON037	410	20	72	204	76	4.4	2.3	bdl	24
ENICON038	105	125	39	128	75	11	1.6	bdl	bdl
ENICON043	1774	192	617	375	151	14	17	1.0	3.1
ENICON044	651	29	176	210	52	2.0	3.3	0.7	57

bdl = below detection limit

Table 10: Platinum-group elements (PGE) concentrations (ppb) in laterite ores and smelter outputs.

Sample	Ru	Rh	Pd	Re	Ir	Pt	Au
ENICON016	23.7	4.0	14.2	bdl	12.1	20.6	2.2
ENICON017	28.3	4.2	7.7	bdl	17.1	18.3	2.1
ENICON020	47.2	8.8	20.3	bdl	22.6	40.9	2.0
ENICON028	26.8	6.2	21.1	bdl	15.4	29.2	3.8
ENICON021	3.4	0.5	bdl	bdl	1.7	2.3	2.3
ENICON022	3.2	0.6	bdl	bdl	1.2	2.6	2.6
ENICON023	632	91.1	255	15.4	365	607	47.1
ENICON024	187	26.0	85.0	39.4	93.4	185	14.6

bdl = below detection limit



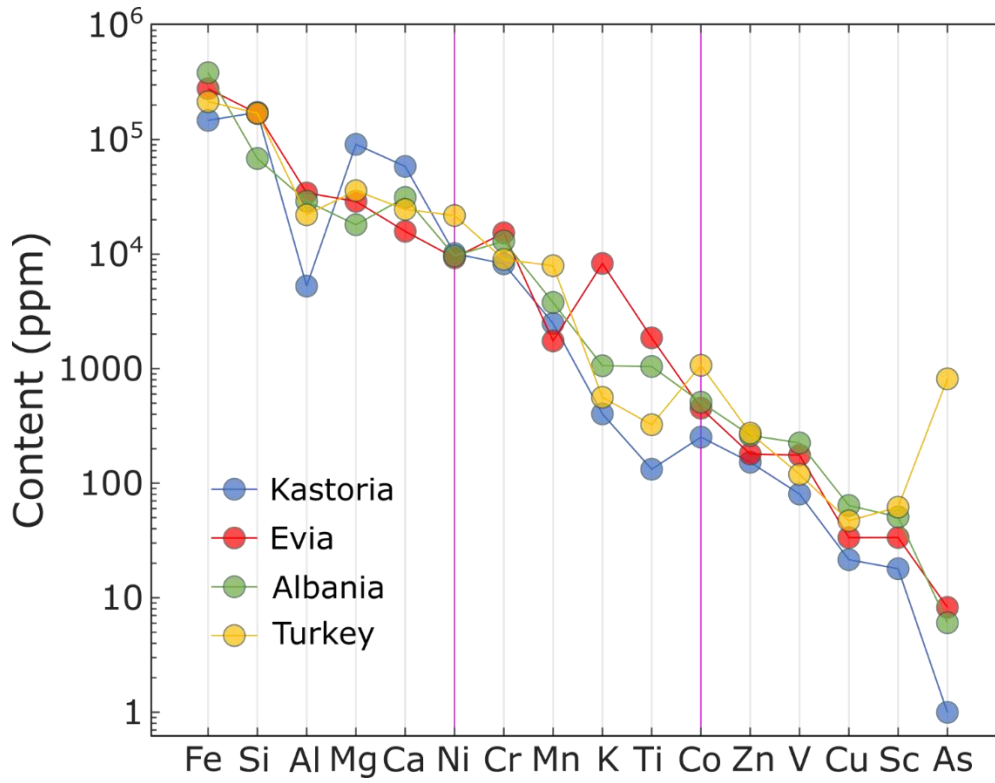


Figure 30: Semi-log line plots showing the concentration of some relevant elements in the ENICON laterite ore samples.



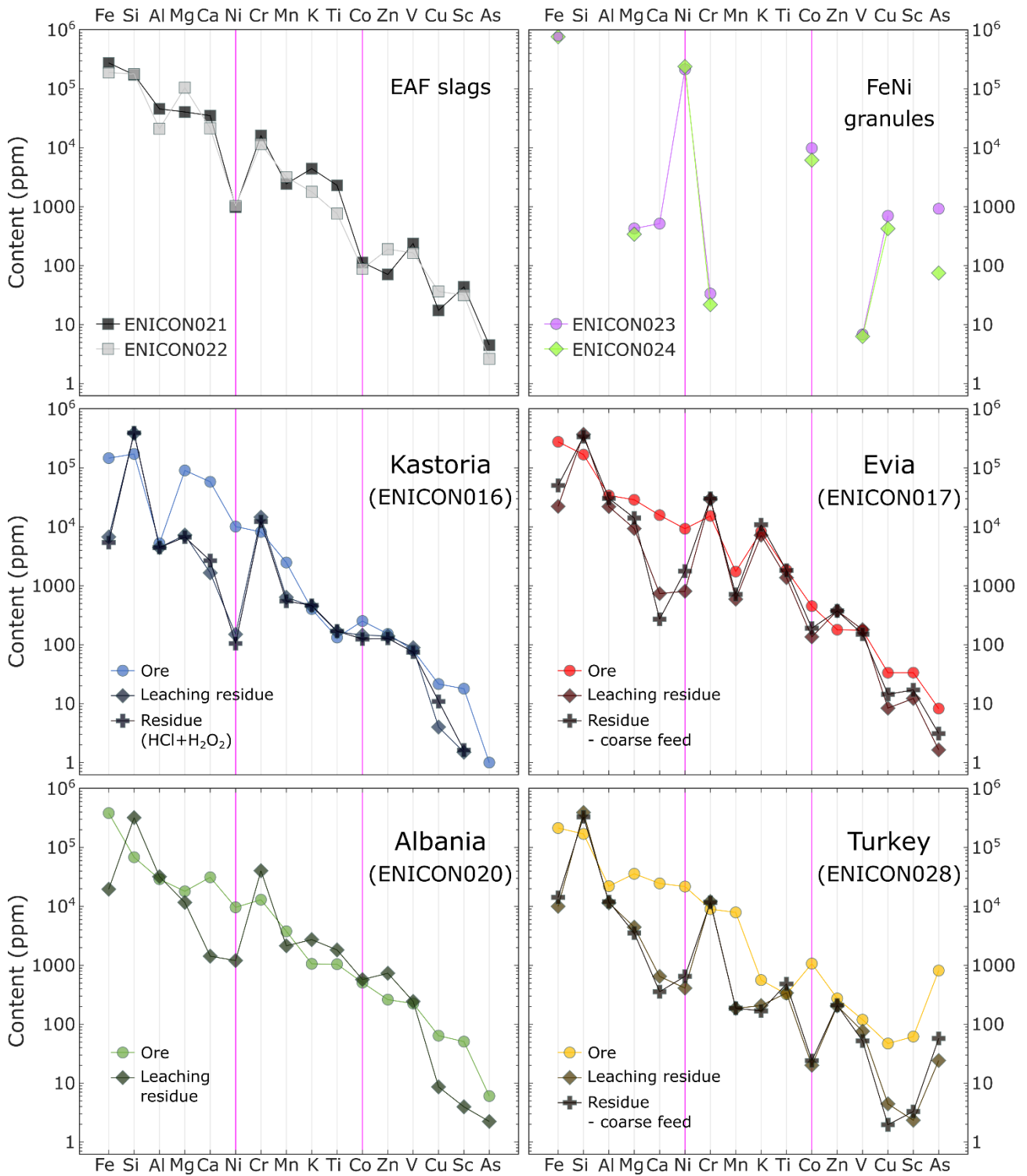


Figure 31: Semi-log line plots showing the concentration of some relevant elements in ENICON laterite-based samples. Missing symbols represent elements below the detection limit.



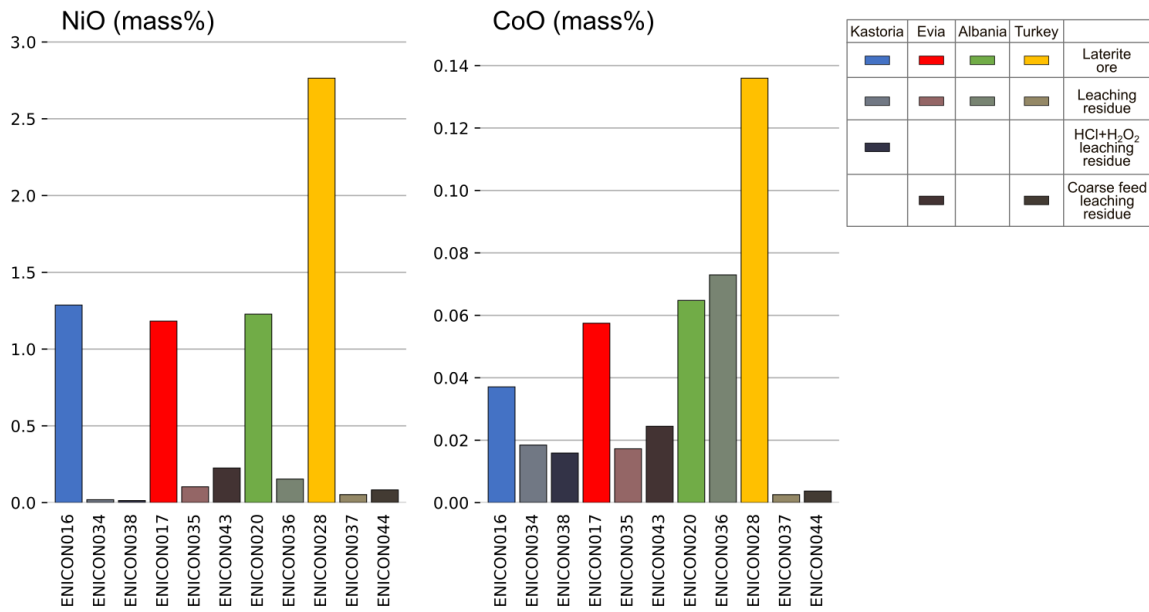


Figure 32: Bar plots showing the bulk concentrations of Ni and Co (oxide mass%) in ENICON laterite-based samples.

3.2.3 Bulk particle size distribution (PSD)

The ROM samples (laterite ores from the stockpile) are the coarsest material investigated, presenting P80 (mark where 80% of particles are smaller than the given value) between 5000 and 7000 μm. The high-grade sample from Turkey (ENICON028) is finer with P80 at around 2000 μm (Figure). The residues after leaching these coarse materials (only carried out for samples ENICON017 and 028) show P80 at around 40 and 100 μm, respectively.

The crushed laterite ore samples present P80 between 200 and 300 μm, and P10 between 0.5 and 1 μm (Figure). Once more, sample ENICON028 shows smaller particle sizes than the other laterites, especially in the coarser range (P80 at 40 μm). The leaching residues are more uniform in size distribution, with P80 between 20 and 40 μm, and P10 between 1 and 3 μm.

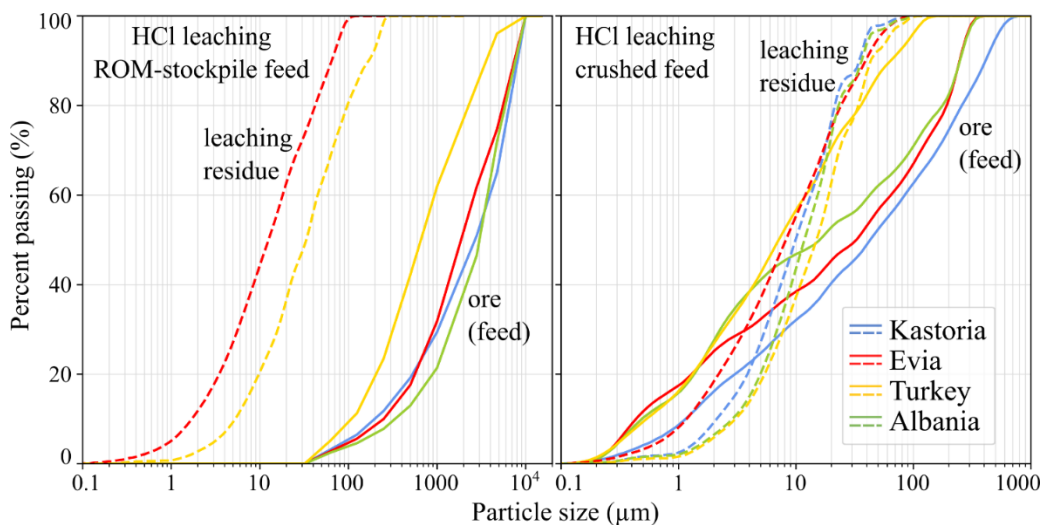


Figure 33: Particle size distribution (PSD) of laterite ores (solid lines) and leaching residues (dashed lines).



3.2.4 Modal mineralogy

The high-grade Ni-bearing minerals (more than 5 mass% of Ni) asbolane (Mn-hydroxide), nimate (Ni-chlorite), and népouite (Ni-serpentine) are mainly present in ENICON028 (the sample with the highest Ni and Co concentration). Asbolane is the only Co-rich mineral phase observed. Although other laterites do not show substantial concentrations of these phases (Figure and



Table 11), they host considerable amounts of Mg-Fe silicates (serpentine group minerals), chlorite, and iron oxyhydroxides (mixed particles of goethite, some hematite, and other iron hydroxides, with a variable degree of crystallinity including amorphous phases), which contain minor amounts of Ni or Co (see section 0). Gangue minerals comprise quartz, carbonates (calcite and dolomite), and phyllosilicates (serpentine, chlorite, talc, and clay minerals) that do not contain nickel.

The leaching residues are largely composed of quartz (70-90%), with chromite and other silicates occurring in variable but often minor proportions.

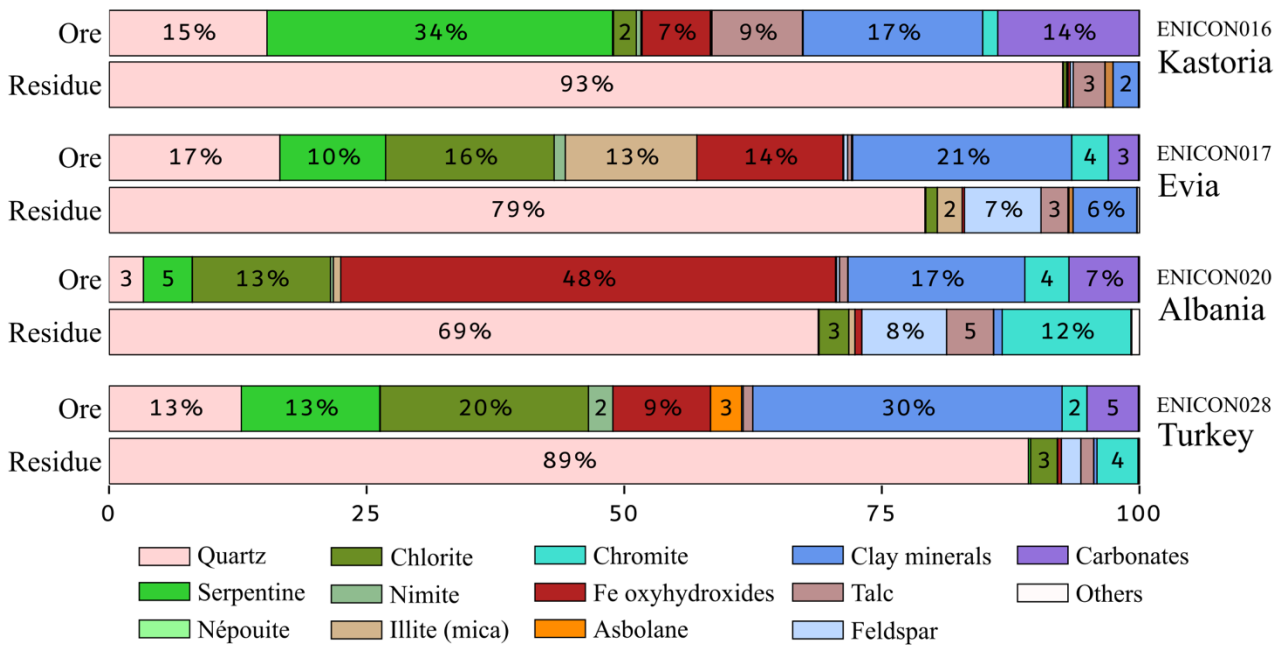


Figure 34: Modal mineralogy of laterite ores and leaching residues obtained by SEM-based automated mineralogy.



Table 11: QEMSCAN output with the modal mineralogy (area%) of the ENICON laterite-based materials.

Mineral	laterites				Smelter slags		HCl Leaching residues				HCl + H ₂ O ₂ Leaching residues	
	Kastoria 016	Evia 017	Albania 020	Turkey 028	Larymna 021	Kavardarci 022	Kastoria 034	Evia 035	Albania 036	Turkey 037	Kastoria 038	Albania 039
quartz	15.32	16.59	3.36	12.85	0.03	0.11	92.55	79.17	68.83	89.21	90.96	67.21
serpentine	42.37	11.22	5.16	16.50			0.70	0.33	0.23	0.35	0.97	0.28
nepouite	0.10	0.00	0.01	0.05			0.001	0.001	0.000	0.000	0.000	0.000
chlorite	2.21	16.36	13.40	20.21	1.80	0.69	0.32	1.12	2.89	2.59	0.36	1.30
nimite	0.45	1.08	0.28	2.37			0.003	0.001	0.004	0.004	0.000	0.010
mica	0.11	12.77	0.72				0.13	2.40	0.59	0.03	0.12	0.57
Fe oxyhydroxides	6.82	14.25	49.16	9.68	5.35	5.43	0.22	0.23	0.71	0.37	0.30	0.79
asbolane	0.07	0.07	0.10	3.01			0.001	0.001	0.004	0.002	0.001	0.003
talc	8.79	0.38	0.81	0.94			3.09	2.61	4.54	1.23	2.85	4.11
smectite	7.95	19.69	16.27	25.38	18.52	5.23	0.12	0.15	0.16	0.15	0.19	0.25
kaolinite				0.85							0.04	1.05
chromite	1.28	3.48	3.14	2.22			2.46	6.19	12.47	3.99	3.66	16.39
feldspar	0.08	0.38	0.28	0.15	0.01	0.06	0.28	7.43	8.23	1.89	0.39	6.73
calcite	13.04	2.61	5.69	0.92	0.04	0.76	0.04	0.04	0.07	0.06	0.04	0.10
dolomite	0.67	0.32	1.05	4.06			0.00	0.00	0.01	0.01	0.00	0.01
apatite	0.000	0.008	0.027	0.012	0.000	0.003	0.000	0.000	0.001	0.000	0.000	0.001
pyrite	0.06	0.11	0.02		0.01	0.14	0.01	0.10	0.03	0.02	0.02	0.03
ilmenite	0.01	0.06	0.04				0.02	0.16	0.38	0.03	0.03	0.51
amphibole	0.64	0.61	0.46	0.72	23.20	19.44	0.02	0.01	0.51	0.03	0.03	0.55
olivine					4.20	55.19						
pyroxene					46.81	12.91						
Others	0.03	0.02	0.03	0.10	0.01	0.04	0.04	0.05	0.36	0.03	0.03	0.11

3.2.5 Mineral grain size

The analyses of average mineral grain sizes show that gangue minerals (quartz and calcite) are relatively coarser than Ni-Co-bearing minerals (Figure). Co-bearing (asbolane and chromite) and Ni-bearing phases (nimite and nepouite, chlorite, serpentine, and Fe oxyhydroxides) are mainly fine-grained (< 50 µm), but largely overlap with other gangue minerals (Table 12).

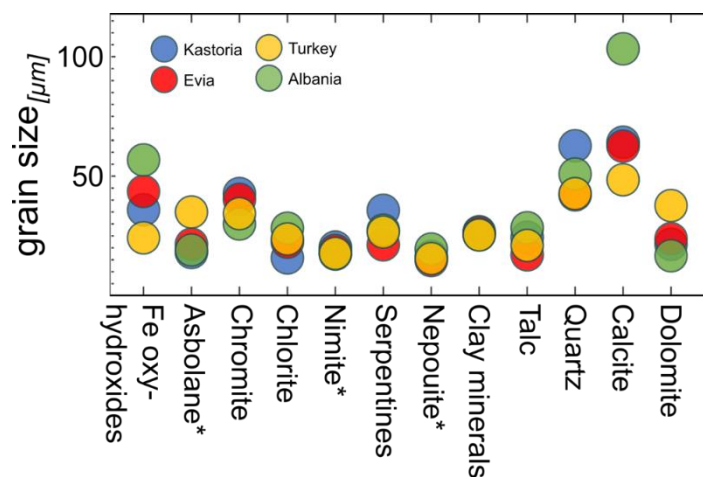


Figure 35: Average grain size of the Ni-Co ore minerals and main gangue minerals observed in the laterite ore samples.



Table 12: QEMSCAN output with the average grain size (μm) of mineral phases identified in the ENICON laterite samples.

Average grain size (μm)				
Mineral	ENICON016 (Kastoria)	ENICON017 (Evia)	ENICON020 (Albania)	ENICON028 (Turkey)
Fe oxyhydroxides ^	35.9	43.6	56.8	24.2
Fe oxyhydroxides (Ni)*	15.2	15.1	15.1	16.5
Fe oxyhydroxides (Ni Mn)*	20.6	17.3	20.5	21.2
Fe oxyhydroxides (Ni Cr)*	20.7	15.3	17.9	22.1
Asbolane*	18.1	21.5	19.1	35.0
Chromite ^	42.7	40.3	30.0	34.3
Chlorite ^	15.8	22.4	28.2	23.7
Nimite*	20.3	18.9	17.4	17.7
Serpentine ^	35.7	21.3	27.4	26.6
Nepouite*	16.4	14.7	19.5	15.5
Quartz	62.7	42.2	50.9	42.7
Feldspar	18.0	22.6	21.0	19.3
Illite	16.2	32.6	25.7	-
Kaolinite	-	-	-	33.6
Fe silicates	26.7	26.4	25.5	25.4
Ca Fe Al silicates	15.8	15.6	18.2	15.4
Ca Mg (Fe) silicates	24.3	17.1	15.7	17.2
Talc	24.4	17.1	28.4	21.0
Calcite	64.2	63.9	103.3	48.5
Dolomite	21.5	23.8	16.7	37.7
Apatite	14.7	22.6	23.9	30.0
Pyrite	42.0	21.8	14.7	-
Ti minerals	18.3	24.9	17.3	-
Others	19.0	16.5	16.3	15.7

* = high-grade ore minerals (major Ni and/or Co phases); ^ = low-grade ore minerals,

3.2.6 Mineral texture and chemistry

Nickel and cobalt occur in variable concentrations in several minerals in the laterite ores (Figure 36). Solid solutions are common in those samples and minerals are combined into groups to facilitate comparison. Only where a clearly distinct compositional group is observed, as in the case of nimite (Ni-chlorite) and népouite (Ni-serpentine), those are distinguished from the main group of chlorite and serpentine, respectively. High-grade Ni and Co phases (> 10% NiO or 5% CoO), represented by asbolane, nimite, and népouite, are only observed in considerable amounts (more than 1%) in the ENICON028 sample. Cobalt is mainly hosted by asbolane, with some contributions from chromite and Fe oxyhydroxides. The chromite in the residues also contains a non-negligible amount of Co (Figure 3737).

The textural features between ore and gangue phases in the laterite ores are quite complex (Figure 38). In many cases, Fe-Co-bearing minerals are associated with gangue minerals or other ore minerals (Figure 39).



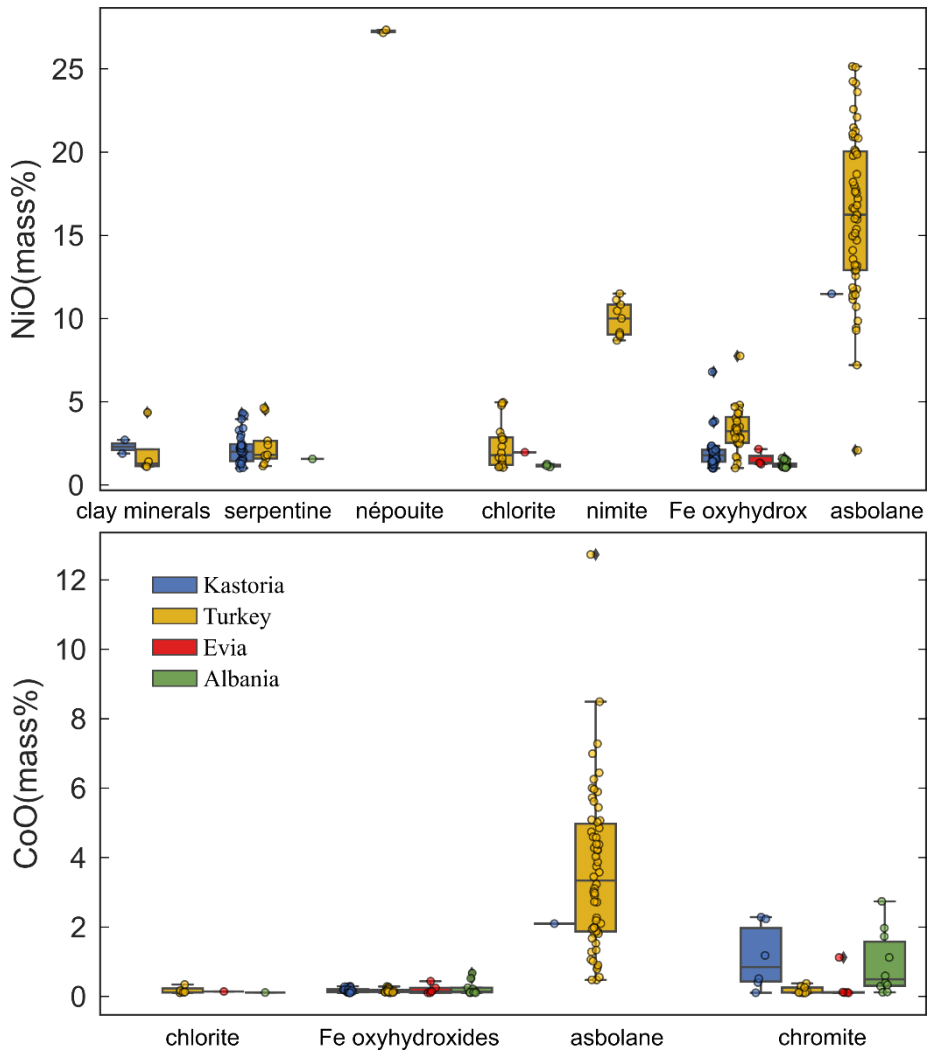


Figure 36: NiO and CoO concentration (mass%) in the ENICON laterite ores. For samples and minerals not shown, the concentration was below the detection limit (around 0.1%) and, therefore, is not reported.

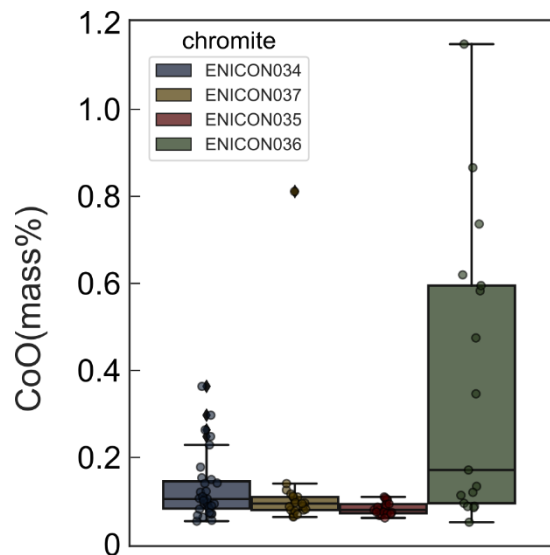


Figure 37: CoO concentration (mass%) in chromite grains in the ENICON leaching residues from laterites.



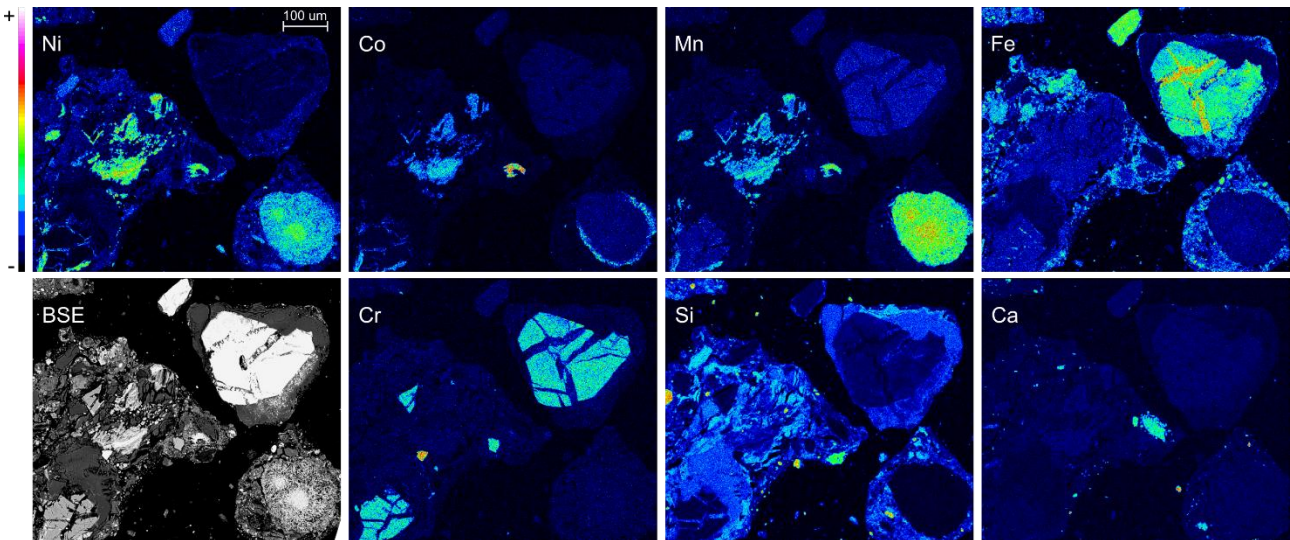


Figure 38: Qualitative WDS elemental maps and reference BSE image (lower left) of Ni-Co-bearing minerals. Example texture of particles containing several mineral grains. The intensity scale (shown on the left) indicates higher values as warmer colours (white as the maximum value) and cooler shades (black as the minimum value) for lower amounts.

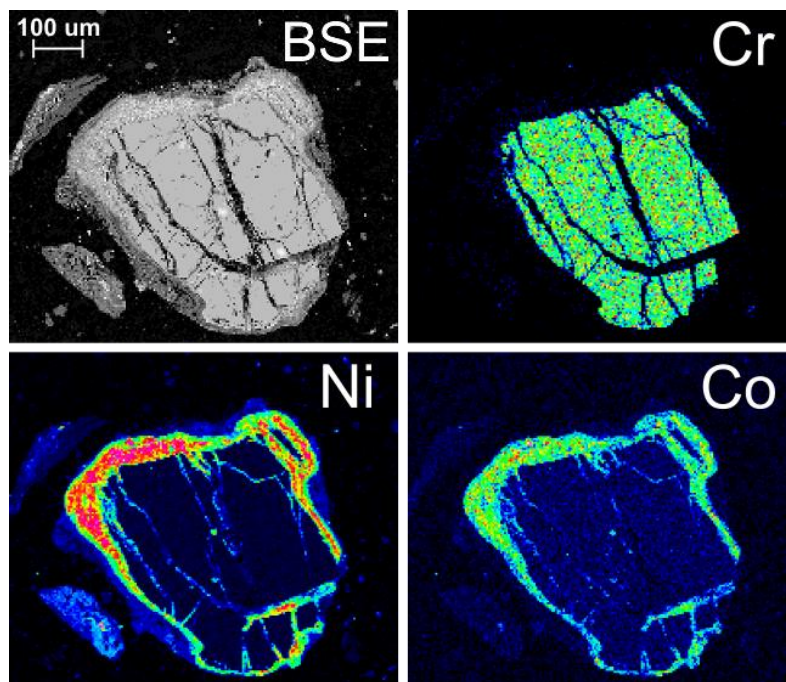


Figure 39: Qualitative WDS elemental maps and reference BSE image (upper left) of asbolane (high Ni and Co phase) surrounding a fractured chromite grain (high Cr phase).

3.2.7 Metal department and mass balance

The department of metals represents the distribution of a given metal in all minerals present in the sample. The calculation of this value considers the concentration of the metal in the mineral, the proportion of this mineral in the sample, and the concentration of metal in the bulk sample. The department is calculated with the following formula:

$$D^i = \frac{(M_k^i * X_k)}{B^i}$$



Where, D^i is the department of element i ; M_k^i is the concentration of element i in mineral k ; X_k is the modal proportion of mineral k ; B^i is the bulk concentration of element i .

In the case of laterite ores, the Ni department is divided between most ore minerals (asbolane, chlorite, serpentine, and Fe oxyhydroxides) but each sample has a dominant ore mineral (Figure 40). Serpentine corresponds to around 67% of the Ni budget in the Kastoria ore (ENICON016). For the Evia ore (ENICON017), chlorite (34%), clay minerals (28%), and serpentine (20%) are the main contributors to Ni budget. The Albanian ore (ENICON020) is the only sample where Fe oxyhydroxides are the main Ni carriers (40%), followed by clay minerals (26%) and chlorite (18%). Lastly, the Turkish ore (ENICON028) shows a more balanced distribution with asbolane as the main Ni carrier (24%) together with chlorite (20%), clay minerals (19%), serpentine and Fe oxyhydroxides (12% each), and nimite (Ni-rich chlorite – 11%).

Cobalt occurs in a limited number of minerals (Figure 40). Chromite is the main Co host in ENICON016 (57%). Although chlorite shows a low CoO concentration (0.1%) it's the main cobalt carrier in sample ENICON017 (62%) due to its high modal proportion (16%). Fe oxyhydroxides are also the main Co host in ENICON020 (69%), whereas for ENICON028 it is asbolane (81%).

The leaching residues retain a Ni department with a similar range of minerals. Nonetheless, in these samples, chlorite is the main Ni carrier in most samples (65-75%), except for ENICON034 (leaching residue of Kastoria ore ENICON016) where serpentine is still the main host of Ni (52%). Contrarily for Co, chromite is almost exclusively the main Co carrier in all residues (>95%).

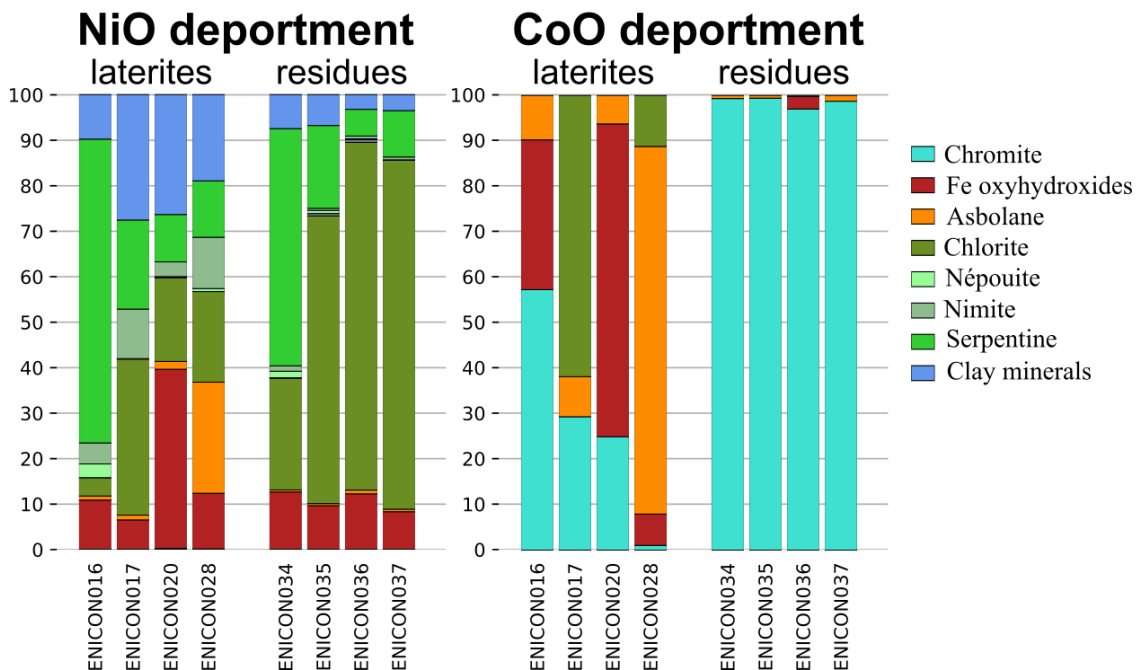


Figure 40: Department of NiO (left) and CoO (right) in the laterite ores and leaching residues.

Considering possible contaminants, the mineralogy is much more diverse than for Ni and Co. Magnesium is distributed between serpentine, clay minerals, and chlorite in the ores, whereas talc and chromite stand out in the residues (Figure 41). Calcium is concentrated in the carbonates (calcite and dolomite) in the ores, whereas feldspar retains this element in the residue (Figure 41). Iron-oxyhydroxides are the main carriers of Fe in the ores, accompanied by chlorite and serpentine (Figure 42). However, chromite, chlorite, and micas host Fe in the residues. Chromium is concentrated by chromite in all samples (Figure 42)



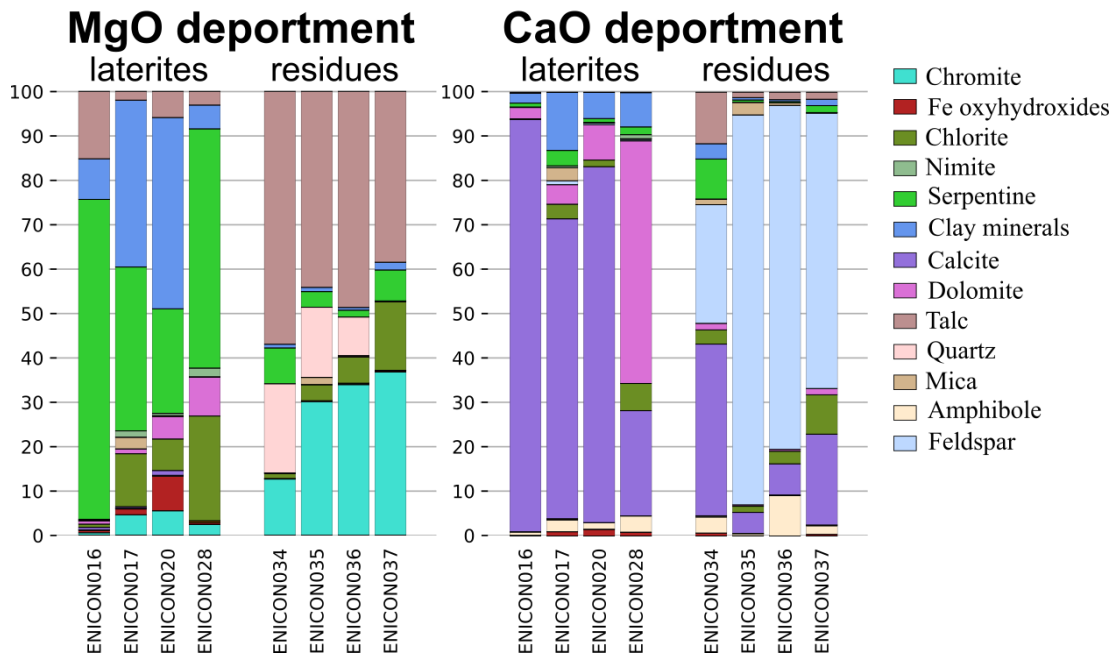


Figure 41: Department of MgO (left) and CaO (right) in the laterite ores and leaching residues.

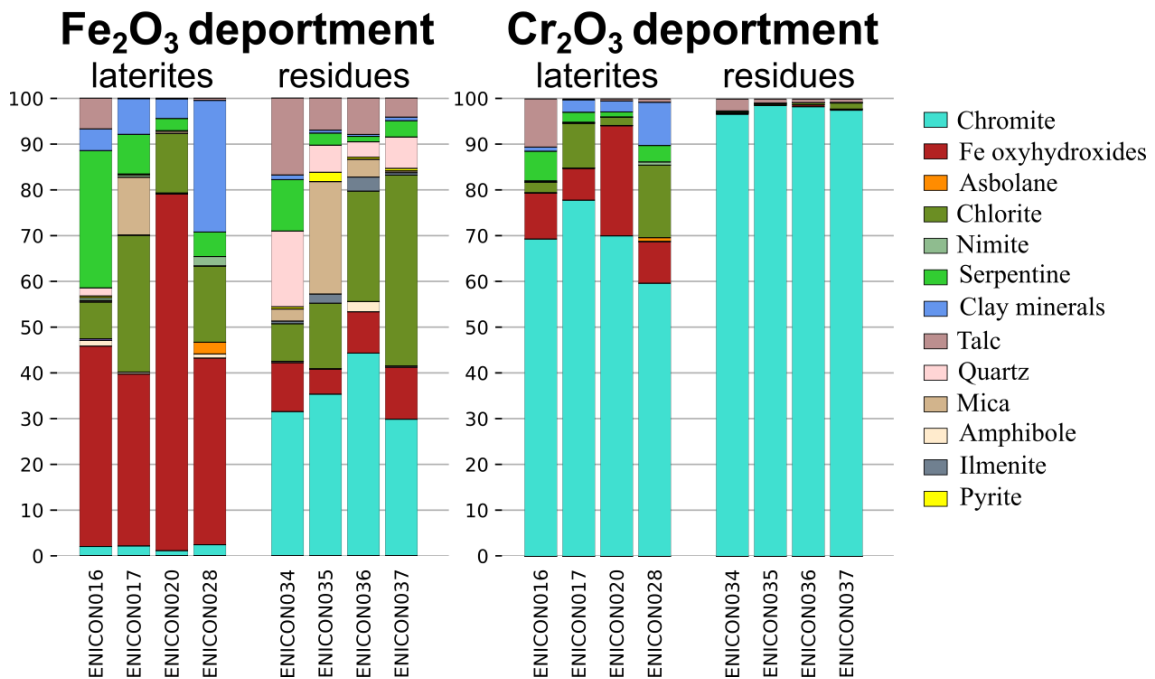


Figure 42: Department of Fe₂O₃ (left) and Cr₂O₃ (right) in the laterite ores and leaching residues.

The geometallurgical mass balance of the leaching flowsheet can be synthesised by the following equation

$$Feed [mass] = Concentrate [mass] + Tailings [mass] \leftrightarrow F = C + T$$

Where the sum of the masses of the products (concentrate, C, and tailings, T) equals the mass of the feed material (F). This equation can be expanded to include the metal grades in each term (marked by non-capitalised letters).

$$F [g] * f [ppm] = C [g] * c [ppm] + T [g] * t [ppm]$$

In the ENICON study cases, the feed is the laterite ore, the concentrate is the pregnant leaching solutions (PLS - metal-rich leachate), and the tailings are the solid residues after leaching. Combining the two equations, if the mass and metal grade in two components is known, the third can be estimated. This



section will thus use the information from the feed and the residues to estimate the values in the PLS (i.e., concentrate).

Table 13: Mass (g) and metal grade (ppm) data for the laterite ores (feed) and leaching residues investigated

Feed sample/Test	Feed mass [g]	Feed Ni grade [ppm]	Feed Co grade [ppm]	Residue mass [g]	Residue Ni grade [ppm]	Residue Co grade [ppm]
ENICON016	1	10113	292	0.3	150	145
ENICON017	1.02	9290	452	0.35	809	136
ENICON020	1	9646	509	0.3	1206	574
ENICON028	1.01	21724	1069	0.38	410	20
ENICON016_ox	1	10113	292	0.3	105	125
ENICON017_coars	143.83	9290	452	64.51	1774	192
ENICON028_coars	185.34	21724	1069	100.22	651	29

Table 14: Estimated values for pregnant leaching solution (PLS) after the HCl ENICON leaching route

Feed sample/Test	PLS mass [g]	PLS Ni grade [ppm]	PLS Co grade [ppm]	PLS Ni grade [g/L]	PLS Co grade [g/L]
ENICON016	0.7	14383	355	1.01	0.02
ENICON017	0.67	13720	617	0.98	0.04
ENICON020	0.7	13263	482	0.93	0.03
ENICON028	0.63	34580	1702	2.33	0.11
ENICON016_ox	0.7	14402	364	1.01	0.03
ENICON017_coars	79.32	15403	663	1.84	0.08
ENICON028_coars	85.12	46536	2294	4.55	0.22

The mass pull or yield (Y) and the mass of metal (M) contained in the products use the equations below:

$$Y [\%] = 100 * \frac{C [g]}{F [g]} = 100 - \left(100 * \frac{T [g]}{F [g]} \right)$$

$$M_F [g] = F [g] * f [ppm]$$

$$M_C [g] = C [g] * c [ppm]$$

$$M_T [g] = T [g] * t [ppm]$$

Lastly, the recovery (R) of metals in the process can be calculated with the following equations:

$$R [\%] = 100 * \frac{M_C [g]}{M_F [g]} = 100 - \left(100 * \frac{M_T [g]}{M_F [g]} \right)$$

Table 15: Estimated metal mass [g] in each product of the HCl leaching of laterite ores and respective metal recoveries and yields

Sample	Ni mass contained in PLS [g]	Co mass contained in PLS [g]	Ni mass contained in residue [g]	Co mass contained in residue [g]	Ni recovery [%]	Co recovery [%]	Mass yield [%]
ENICON016	0.0101	0.00025	0.00005	0.00004	99.6	85.1	70.0



ENICON017	0.0092	0.00041	0.0003	0.00005	97.0	89.7	65.7
ENICON020	0.0093	0.00034	0.0004	0.00017	96.3	66.2	70.0
ENICON028	0.0218	0.00107	0.0002	0.00001	99.3	99.3	62.4
ENICON016_ox	0.0101	0.00027	0.00002	0.00002	99.8	91.4	80.0
ENICON017_coars	1.2217	0.05262	0.1144	0.01239	91.4	80.9	55.1
ENICON028_coars	3.9611	0.19529	0.0652	0.00291	98.4	98.5	45.9

When comparing different tests, it is better to use the calculated metal recoveries and mass yield instead of comparing the metal masses in the products. The latter depends on the mass of the feed, thus tests with larger masses of feed should produce larger amounts of metals in the products regardless of the effectiveness of the process.

In the study cases, the recoveries of Ni are always considerably higher than those of Co (Table 15). The only exception is for the saprolitic laterite from Turkey (ENICON028), where the recoveries of Ni and Co are very similar. One interpretation of this is that, in most samples, the Ni-bearing and Co-bearing minerals present different leachabilities, with the latter harder to dissolve in HCl. Conversely, in ENICON028, ore minerals behave similarly, and more specifically, asbolane contains a high content of both Ni and Co, which are equally released once it dissolves. The Co recovery in sample ENICON020 is significantly worse than in all other samples. The main difference in this sample is the large amount of Fe oxyhydroxides in the ore feed (48%) and the high amount of chromite (12%) in the leaching residue (Figure). This suggests that chromite is being concentrated in the leaching residue and restraining a considerable part of Co in it.

Furthermore, the recoveries of the leaching tests using the crushed feed are higher than in the tests with the coarse feed. This shows that the leaching is more effective in finer feeds, which is expected since smaller particles have a higher surface area/volume ratio. However, the mass yield of the leaching of coarse feeds is much smaller than that of the crushed feeds. A lower mass yield indicates that the concentrate (PLS) has a smaller mass (i.e., higher concentration and “cleaner” concentrates), which suggests that leaching was more selective in the tests with the coarse feed. Especially for sample ENICON028, recoveries at around 98% with a mass yield of 46% in the coarse feed leaching perform well against recoveries at 99% with a mass yield of 62% for the crushed feed. Conversely, for ENICON017, recoveries of 91% for Ni and 81% for Co with a mass yield of 55% in the coarse feed are less effective than recoveries of 97% for Ni and 90% for Co with a mass yield of 66% in the crushed feed.

Overall, the efficiency of any process depends on the mineral properties of the ore. Therefore, it is necessary to assess how much metal is present in each mineral. The feed mass was normalized to 1 kg to allow the comparison between different tests. This approach should only be considered an estimate because of the reasons mentioned earlier and upscaling leaching tests may not present a linear increase in the grades. Once the metal content in the bulk samples and the metal department in mineral phases are all known, it is possible to calculate the metal content of each mineral phase in the samples.

$$M_{min} [g] = M_{bulk} [g] * D [%]$$



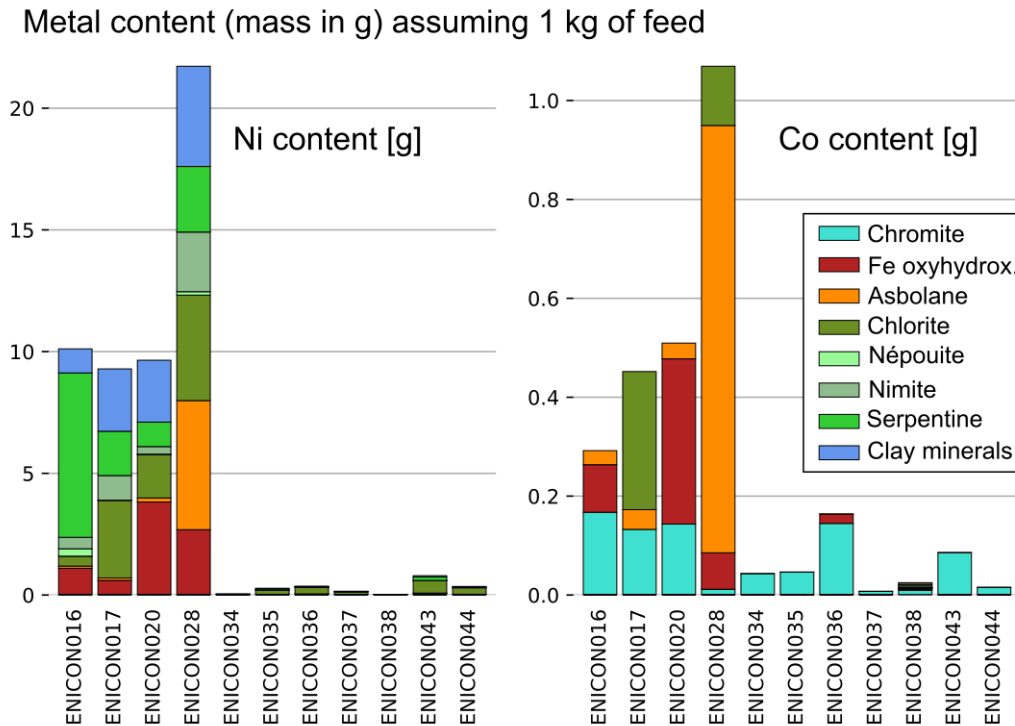


Figure 43: Estimated Ni and Co contents [g] in the ENICON laterite ores and leaching residues after normalization by assuming a uniform mass of 1 kg for all feeds. The total height of the bars indicates the bulk amount of metal in each sample, whereas the colored sections represent the contribution of each mineral.

This assumption gives an estimate of possible target minerals and problematic phases in the process. For nickel, the amount of metal left in the residue is very minor (Figure 4) as expected from the high recoveries calculated. It is mostly controlled by chlorite in the residue, suggesting that this phase is not fully dissolved in the leaching process. The residues of tests with a crushed feed present smaller contents of metals than those carried out with the coarse feeds. For cobalt, the amount of Co-bearing chromite left after leaching is significant and effectively traps this metal in the residue.

4 Future activities

Further geochemistry and mineralogy on samples that were unable to be obtained prior to this report may be collected at a later date, where possible. The mass balance can be improved with more information from the large-scale leaching tests. This can then be assessed in line with the life cycle and economic-environmental assessment (LCA-TEA – WP5). With all the information from the final flowsheet, the geometallurgical protocol can be refined and assessed more thoroughly.

5 Implications and Conclusions

The HCl leaching route developed in the ENICON project for processing sulphidic and lateritic ores has given mixed, but mostly positive, results. An additional combination of acidic and oxidizing leaching has also been tested for the sulphidic ore samples, with positive results.



The combination of acidic and subsequent oxidative leaching has been effective in removing a large amount of the iron of the sample by targeting pyrrhotite, without significant loss of metals of interest in the first phase (acidic leaching) and extraction of Ni and Co in the subsequent phase (oxidizing leaching), as seen through bulk geochemistry and modal mineralogy. Changes in iron speciation as seen through XPS, further suggests the chemical changes after leaching. Work on the SEM and automated mineralogy show that there are some sulphides of interest (e.g. pentlandite) in the residues. The HCl leaching, however, had mixed results. While the processing of the high S tailings was relatively effective in extracting nickel and cobalt from the sulphides (residual Fe-Ni sulphides/sulphates <1%), the retrieval for the Ni concentrate was much lower. In that case, the remaining Fe-Ni sulphide/sulphates was above 18%, reflected in the concentration of Ni > 7 wt.%; similar results were seen for cobalt. It is possible that the initial amount of sulphides in this sample (> 60%) was a limiting factor in the success of the extraction in the conditions proposed by WP2.

The process, when applied to samples from laterite deposits, is effective in extracting nickel from the ores. However, for cobalt, the picture is slightly more complicated. Both bulk geochemical and mineralogical data suggest that nickel-bearing ore minerals (Mg-Fe phyllosilicates, mainly serpentine, chlorite, and clay minerals), and oxide-hydroxides, mainly asbolane and Fe oxyhydroxides) are dissolved during the HCl leaching stage. Therefore, nickel is quantitatively extracted from the mineral structures and reports to the leachate solution. Contrarily for Co-containing minerals, oxide-hydroxides effectively dissolve during leaching, but chromite is not attacked by HCl at the experimental conditions. Chromite contains up to 2.5% CoO (median at about 0.5%), thus retaining some of the cobalt in the solid residue. This interpretation correlates with the predominance of SiO₂ and Cr₂O₃ in the composition of the leaching residues and the occurrence of large amounts of quartz and chromite in these samples. Accordingly, all the elements hosted by chromite (Cr, Zn, V, and Co) report to the leaching residue and do not allow their quantitative recovery. To effectively extract both nickel and cobalt from laterite ores, the leaching of chromite in harsher conditions is required.

The leaching of crushed material seems to provide a better recovery of metals, especially in samples that contain a large array of ore minerals. However, the cost of this extra grinding stage should be assessed against the lower metal recovery in the leaching using a coarser feed.

Additionally, a beneficiation stage (ore upgrading) before leaching should improve the recovery of interest metals. The coarser grain size of quartz and carbonates in the laterite ores provides a cheap and easy solution to remove these gangue phases by a sieving/screening step without significantly affecting the ore minerals. This should decrease the mass of the leaching feed and remove carbonates, which are heavy acid consumers, possibly increasing the leaching efficiency and metal recovery.

6 References

- Andersen, J.C.Ø., Rollinson, G., Snook, B., Herrington, R., Fairhurst, R.J., 2009. Use of QEMSCAN® for the characterization of Ni-rich and Ni-poor goethite in laterite ores. *Minerals Engineering* 22, 1119–1129. <https://doi.org/10.1016/j.mineng.2009.03.012>
- Barnes, S-J. and Lightfoot, P.C. 2005. Formation of magmatic nickel-sulfide ore deposits and processes affecting their copper and platinum-group element contents. In Hedenquist, J.W., Thompson, J.F.H., Goldfarb, R.J. and Richards, J.P. (eds.) *Economic Geology 100th Anniversary Volume*, p. 179-213.
- Bartzas, G., Komnitsas, K., 2024. Cradle to gate life-cycle assessment of battery grade nickel sulphate production through high-pressure acid leaching. *Science of The Total Environment* 952, 175902. <https://doi.org/10.1016/j.scitotenv.2024.175902>



- Bartzas, G., Komnitsas, K., 2015. Life cycle assessment of ferronickel production in Greece. *Resources, Conservation and Recycling* 105, 113–122. <https://doi.org/10.1016/j.resconrec.2015.10.016>
- Bates, R.L. and Jackson, J.A. 1987. *Glossary of Geology*. Third edition. *Glossary of Geology. Third edition* 754p.
- Butt, C.R.M., Cluzel, D., 2013. Nickel Laterite Ore Deposits: Weathered Serpentinites. *Elements* 9, 123–128. <https://doi.org/10.2113/gselements.9.2.123>
- Davidson, C. M., Duncan, A. L., Littlejohn, D., Ure, A. M., & Garden, L. M. 1998. A critical evaluation of the three-stage BCR sequential extraction procedure to assess the potential mobility and toxicity of heavy metals in industrially-contaminated land. *Analytica Chimica Acta*, 363(1), 45-55.
- Elias, M., 2002. Nickel laterite deposits – geological overview, resources and exploitation (CODES Special Publication, 4), Giant ore deposits: Characteristics, genesis and exploration. CODES.
- Gleeson, S.A., Herrington, R.J., Durango, J., Velásquez, C.A., Koll, G., 2004. The Mineralogy and Geochemistry of the Cerro Matoso S.A. Ni Laterite Deposit, Montelíbano, Colombia. *Economic Geology* 99, 1197–1213.
- González-Pérez, I., Gervilla, F., González-Jiménez, J.M., Kojonen, K. 2021. Genesis of an exotic platinum-group-mineral-rich and Mg-poor chromitite in the Kevitsa Ni-Cu-platinum-group-elements deposit. *Mineralogy and Petrology*, 115(5), pp. 535–555. Available at: <https://doi.org/10.1007/S00710-021-00751-1/TABLES/2>.
- Gregoir, L., Van Acker, K., 2022. Metals for Clean Energy: Pathways to solving Europe’s raw materials challenge (Policymaker summary). *Eurometaux*.
- Gupta, J.G.S., 1994. CHARACTERIZATION OF MAJOR, MINOR AND TRACE ELEMENTS IN SIX CCRMP (TDB-1, WGB-1, UMT-1, WPR-1, WMG-1 AND WMS-1) AND ONE IWG (ZW-C) GEOCHEMICAL CANDIDATE REFERENCE MATERIALS. *Geostandards Newsletter* 18, 111–122. <https://doi.org/10.1111/j.1751-908X.1994.tb00510.x>
- Horn, S., Gunn, A.G., Petavratzi, E., Shaw, R.A., Eilu, P., Törmänen, T., Bjerkgård, T., Sandstad, J.S., Jonsson, E., Kountourelis, S., Wall, F., 2021. Cobalt resources in Europe and the potential for new discoveries. *Ore Geology Reviews* 130, 103915. <https://doi.org/10.1016/j.oregeorev.2020.103915>
- IEA, 2021. *The Role of Critical Minerals in Clean Energy Transitions*, World Energy Outlook Special Report. OECD Publishing, Paris.
- Jessup, A., Mudd, G.M., 2008. Environmental Sustainability Metrics fkonor Nickel Sulphide Versus Nickel Laterite, in: *Blueprints for Sustainable Infrastructure*. Presented at the 3rd International Conference on Sustainability Engineering & Science, Auckland, New Zealand.
- Luolavirta, K., Hanski, E., Maier, W., & Santaguida, F. 2018a. Whole-rock and mineral compositional constraints on the magmatic evolution of the Ni-Cu-(PGE) sulfide ore-bearing Kevitsa intrusion, northern Finland. *Lithos*, 296–299, 37–53. <https://doi.org/10.1016/j.lithos.2017.10.015>
- Luolavirta, K., Hanski, E., Maier, W., Santaguida, F., 2018b. Characterization and origin of dunitic rocks in the NI-CU-(PGE) sulfide ore-bearing kevitsa intrusion, northern finland: Whole-rock and mineral chemical constraints. *Bulletin of the Geological Society of Finland* 90, 5–32. <https://doi.org/10.17741/bgsf/90.1.001>
- Makkonen, H. V., Halkoaho, T., Konnunaho, J., Rasilainen, K., Kontinen, A., Eilu, P., 2017. Ni-(Cu-PGE) deposits in Finland – Geology and exploration potential. *Ore Geol Rev* 90, 667–696. <https://doi.org/10.1016/J.OREGEOREV.2017.06.008>



- Mudd, G.M., 2010. Global trends and environmental issues in nickel mining: Sulfides versus laterites. *Ore Geology Reviews* 38, 9–26. <https://doi.org/10.1016/j.oregeorev.2010.05.003>
- Mudd, G.M., Jowitt, S.M., 2022. The New Century for Nickel Resources, Reserves, and Mining: Reassessing the Sustainability of the Devil's Metal. *Economic Geology* 117, 1961–1983. <https://doi.org/10.5382/econgeo.4950>
- Mudd, G.M., Jowitt, S.M., 2014. A Detailed Assessment of Global Nickel Resource Trends and Endowments. *Economic Geology* 109, 1813–1841. <https://doi.org/10.2113/econgeo.109.7.1813>
- Musuku, B., Muzinda, I., Lumsden, B., 2016. Cu–Ni processing improvements at First Quantum's Kevitsa mine. *Miner Eng* 88, 9–17. <https://doi.org/10.1016/J.MINENG.2015.08.005>
- Mutanen, Tapani., 1997. Geology and ore petrology of the Akanvaara and Koitelainen mafic layered intrusions and the Keivitsa-Satovaara layered complex, northern Finland. *Geological Survey of Finland. Bulletin* 395, 233p.
- Naldrett, A.J., 2004. Magmatic Sulfide Deposits. *Magmatic Sulfide Deposits*. <https://doi.org/10.1007/978-3-662-08444-1>
- Stanković, S., Martin, M., Goldmann, S., Gäbler, H.-E., Ufer, K., Haubrich, F., Moutinho, V.F., Giese, E.C., Neumann, R., Stropper, J.L., Stummeyer, J., Kaufhold, S., Dohrmann, R., Oxley, A., Marbler, H., Schippers, A., 2022. Effect of mineralogy on Co and Ni extraction from Brazilian limonitic laterites via bioleaching and chemical leaching. *Minerals Engineering* 184, 107604. <https://doi.org/10.1016/j.mineng.2022.107604>
- Tupaz, C.A.J., Watanabe, Y., Sanematsu, K., Echigo, T., 2020. Mineralogy and geochemistry of the Berong Ni-Co laterite deposit, Palawan, Philippines. *Ore Geology Reviews* 125, 103686. <https://doi.org/10.1016/j.oregeorev.2020.103686>
- USGS, 2024. Nickel - Mineral Commodity Summary. United States Geological Survey.
- Vandenbergh, R.E., De Resende, V.G., Da Costa, G.M., De Grave, E., 2010. Study of loss-on-ignition anomalies found in ashes from combustion of iron-rich coal. *Fuel* 89, 2405–2410. <https://doi.org/10.1016/j.fuel.2010.01.022>
- Villanova-de-Benavent, C., Proenza, J.A., Galí, S., García-Casco, A., Tauler, E., Lewis, J.F., Longo, F., 2014. Garnierites and garnierites: Textures, mineralogy and geochemistry of garnierites in the Falcondo Ni-laterite deposit, Dominican Republic. *Ore Geology Reviews* 58, 91–109. <https://doi.org/10.1016/j.oregeorev.2013.10.008>
- Watling, H.R., Elliot, A.D., Fletcher, H.M., Robinson, D.J., Sully, D.M., 2011. Ore mineralogy of nickel laterites: controls on processing characteristics under simulated heap-leach conditions. *Australian Journal of Earth Sciences* 58, 725–744. <https://doi.org/10.1080/08120099.2011.602986>

